3 1176 00159 3293

CLASS

NACA

of *H. L. Dryden* Date 6-11-53
per naca Release form #1521. By HAR, 7-21-53.

RESEARCH MEMORANDUM

PRESSURE-DISTRIBUTION AND RAM-RECOVERY CHARACTERISTICS

OF NACA SUBMERGED INLETS AT HIGH SUBSONIC SPEEDS

By Joseph L. Frank

Ames Aeronautical Laboratory
Moffett Field, Calif.

NATIONAL ADVISORY COMMITTEE
FOR AERONAUTICS
WASHINGTON
July 7, 1950

NATIONAL ADVISORY COMMITTEE FOR AERONAUTICS

RESEARCH MEMORANDUM

PRESSURE-DISTRIBUTION AND RAM-RECOVERY CHARACTERISTICS OF NACA

SUBMERGED INLETS AT HIGH SUBSONIC SPEEDS

By Joseph L. Frank

SUMMARY

This report presents ram-recovery and mass-flow ratios for NACA sub-
merged inlets at four positions on the fuselage of a model of a hypothet-
ical fighter airplane. Ram-recovery and mass-flow contours in the inlet
and plots of the pressure distribution over the ramp and in the inlet
entrance are shown for the rearmost inlet position. The Mach number range
was from 0.30 to 0.875, and the angle-of-attack range was from $-2°$ to $12°$.

Ram-recovery ratios were generally maximum for mass-flow ratios
between 0.60 and 0.80 for all inlet positions. The inlet in the most for-
ward position provided the highest ram-recovery ratios for almost every
test condition, ram-recovery ratios as high as 0.94 being measured for
this position. Ram-recovery ratio at the inlet in the second location
was satisfactory, averaging 0.025 lower than that of the forward inlet.
At the two rear positions, ram-recovery ratio diminished rapidly as the
Mach number was increased beyond 0.70 and the angle of attack was increased
above $0°$.

INTRODUCTION

Tests were conducted in the Ames 16-foot high-speed wind tunnel to
continue investigation, at higher subsonic Mach numbers, of NACA submerged
inlets developed in the Ames 7- by 10-foot wind tunnels as discussed in
references 1 and 2. For the tests in the 16-foot wind tunnel, the inlets
were mounted at four longitudinal locations on a model of a hypothetical
fighter airplane. Results of tests in the 16-foot wind tunnel for inlets
in the most forward position on the fuselage and with boundary-layer deflec-
tors were reported in reference 3 with the presentation of ram-recovery
ratios, mass-flow ratios, and pressure distribution. Results for inlets
at four positions on the fuselage (with and without boundary-layer
deflectors) were reported in reference 4 with the presentation of ram-
recovery ratios and mass-flow ratios. To expedite release, reference 4
presented ram-recovery and mass-flow ratios computed from pressure data

CONFIDENTIAL

averaged during the tests by an integrating manometer. The present report presents ram-recovery and mass-flow ratios computed from the data used in reference 4, but computed by the method of reference 3, which yields more precise values of pressure recovery. Ramp and inlet static-pressure distribution and contours of local ram-recovery and local mass-flow ratios in the inlet mounted in the rearmost position are also presented.

SYMBOLS

The symbols used in this report and their definitions are as follows:

H effective total pressure, pounds per square foot

M Mach number

P pressure coefficient $\left(\dfrac{p - p_o}{q_o} \right)$

P_{cr} critical pressure coefficient (the pressure coefficient corresponding to local sonic velocity)

p static pressure, pounds per square foot

q dynamic pressure, pounds per square foot

α_u angle of attack uncorrected for tunnel-wall effects (measured relative to the fuselage reference line), degrees

$\dfrac{H - p_o}{H_o - p_o}$ ram-recovery ratio

$\dfrac{m}{m_o}$ mass-flow ratio (the ratio of the mass flow through a unit inlet area to the mass flow through a unit area in the free stream)

Subscripts

o free stream

1 duct entrance

APPARATUS

A complete description of the model is given in reference 3. The model (shown in figs. 1 and 2) represented a hypothetical fighter airplane.

Throughout the tests a pair of identical inlets was used. They were disposed symmetrically on each side of the fuselage and were connected to a common plenum chamber in the rear part of the fuselage. The fuselage stations mentioned throughout this report are expressed in inches from the fuselage nose. The four longitudinal inlet locations investigated (fig. 2) were at fuselage stations 34.25, 42.50, 50.75, and 59.00 and corresponded, respectively, to 16.7 percent of the root chord ahead of and 8.3, 33.3, and 58.3 percent of the root chord behind the wing-root leading edge. Dimensions of the ramp and the lip are shown in figure 3. The ramp angle (7°) and the ramp length (21.10 in.) remained constant for all inlet locations. Due to the difference in fuselage shape at the various ramp locations, the curvature at the beginning of the ramp was different for the various locations. During all parts of the investigation covered in this report, the angle of the inlet lip (fig. 3) was -3°.

Internal pressures (from which pressure losses and flow rates were calculated) were measured with a rake in the duct 2.1 inches behind the lip leading edge. The rake consisted of 30 total-pressure and 30 static-pressure tubes. Location of the pressure tubes on the rake is shown in figure 4. Orifices to measure pressure distribution were located along the ramp center line and along the walls of the ramp. These rows of orifices extended past the inlet into the duct.

TESTS

Range of tests

During the tests the Mach number was varied from 0.30 to 0.875. The Reynolds numbers per foot of length corresponding to these Mach numbers were 2.0 and 3.9 million, respectively. In general, the angle-of-attack range of the tests was from -2° to 12°, except where the strength of the model limited the angle of attack. The mass-flow ratio was varied from 0 to 1.80, the upper and lower limits depending upon pressure recovery and flow instability, respectively. With the lowest total mass-flow rate for both inlets, flow instability forced most of the air to flow into one or the other of the inlets. Data for the low mass-flow ratios were not obtained at some angles of attack because most of the flow usually entered the inlet in which the measurements were taken. At a Mach number of 0.875, mass-flow ratios above approximately 0.90 were not obtained, probably because of choking in the internal ducts.

Data Corrections

The Mach number calibration for the tests was derived from a survey of the wind tunnel without the model in place and was corrected for

constriction effects due to the presence of the model by the method of reference 5. No other corrections were made to the data for tunnel-wall effects. The uncorrected angle of attack of the model is estimated to be about 10 percent smaller than it would be in free air for the same lift on the wing.

Calculation of Ram-Recovery and Mass-Flow Ratios

To expedite release of reference 4, ram-recovery and mass-flow ratios were computed from data recorded by an averaging manometer, this manometer supplying the arithmetical average of readings of 30 total-pressure tubes and the arithmetical average of the readings of 30 static-pressure tubes. However, the average total pressure supplied by the averaging manometer was not a correct measure of the stream total energy; for this reason the results of the same tests were recomputed for the present report by more exact methods discussed below.

The effective total pressure H used in the present report for computing ram-recovery ratio represents the total energy per unit mass passing a given section, in this case a station 2.1 inches behind the leading edge of the inlet lip. To correctly reflect the local total energy in the area assigned to each of 30 total-pressure tubes, the logarithm of the total pressure at each of the tubes was weighted by the mass flow through the area assigned to that tube in accordance with the method developed in reference 3. The logarithm of the effective total pressure was then calculated by dividing the summation of these weighted values by the total mass flow through the inlet.

Mass flows were computed for the areas assigned to each of the 30 total-pressure tubes; the mass-flow ratio for the entire duct was then computed from the summation of these 30 local mass flows.

In contrast to the method of calculation of ram-recovery ratio used in the present report, the averaging-manometer method used in reference 4 employs a total pressure averaged directly from the readings of the total-pressure tubes, there being no weighting for the mass flow through the area assigned to each tube.

A comparison of data computed by the two different methods revealed that ram-recovery ratios computed by the more exact method of weighting the total pressures were consistently higher than those computed by the shorter averaging-manometer method. Ram-recovery ratios computed by the more exact method averaged approximately 0.044 higher at 0.60 mass-flow ratio and approximately 0.024 higher at 0.80 mass-flow ratio. Below a mass-flow ratio of approximately 0.88, mass-flow ratios computed by the more exact method were lower; above this point, they were higher.

RESULTS AND DISCUSSION

The variation of ram-recovery ratio with mass-flow ratio for various Mach numbers and angles of attack is shown in figures 5 through 8. Figure 9, cross-plotted from figures 5 through 8, presents the variation of ram recovery with angle of attack and with Mach number. Figure 10 presents contours of local ram-recovery and mass-flow ratios for the inlet in the rearmost location. Figures 11 through 24 present the pressure distribution along the ramp and walls of the inlet for the rearmost location.

Effect of Mass-Flow Ratio

In general, the shapes of the curves of ram-recovery variation with mass-flow, shown in figures 5 through 8, were similar for all inlet locations, Mach numbers, and angles of attack. The general pattern was a sharp rise in ram recovery as mass flow was increased from the lowest values to approximately 0.60, a leveling off and maximum ram recovery between 0.60 and 0.80 mass-flow ratio, and a dropping off of ram-recovery ratio above 0.80 mass-flow ratio. Thus, it is seen that the region for most efficient operation of the inlet tested, as indicated by pressure measurements 2.1 inches behind the lip leading edge, was between 0.60 and 0.80 mass-flow ratio. The cross plots shown in figure 9 were made at 0.60 and 0.80 mass-flow ratios, the region of maximum ram recovery.

Effect of Inlet Location

As indicated in figure 9, the inlet in the most forward location provided the highest ram recovery in all except a few instances where recovery at the inlet in the second location was equal. This superior performance of the most forward inlet was to be expected, as reference 4 showed that the boundary layer was relatively thin along the forward portion of the fuselage. The maximum ram-recovery ratio at the forward inlet was 0.94 for a Mach number of 0.60, an angle of attack of -2°, and a mass-flow ratio of approximately 0.70 (fig. 5). Ram recovery of the inlet in the second location was satisfactory, averaging 0.025 lower than that of the forward inlet. The maximum difference between ram-recovery ratios for the two forward locations for similar test conditions was 0.035.

Inlets at the third and fourth locations (from the nose) maintained satisfactory ram-recovery ratios at Mach numbers below 0.70 and angles of attack near 0°, averaging only 0.03 and 0.04, respectively, below those of the most forward position. However, as Mach number was increased beyond 0.70 and angle of attack was increased above 0°, ram recovery at the two rear inlets decreased rapidly. The progressively poorer ram recovery (as the inlet was moved aft) was due mainly to two factors.

The first factor was the growth in thickness of the boundary layer
along the fuselage, the boundary layer at the rearmost inlet location being
at least twice as thick as that at the forward inlet location. The con-
tours of local ram-recovery ratio, presented in figure 10, show the areas
of low ram recovery in the rearmost inlet. The contours in figures 10(n),
10(o), and 10(s) show the large losses present at the outer corners of the
inlet when operating with high mass flows. These losses are believed to
have been due, in part, to the boundary-layer air that spilled over the
outer edges of the ramp walls and flowed into the corners of the inlet.

The second factor causing progressively poorer ram recovery as the
inlet was moved aft was the velocities induced by the wing. Local veloc-
ities induced by the wing resulted in supersonic speeds (and consequent
shock-wave formation) at a lower free-stream Mach number for the rear
inlet locations than for the forward locations. Evidence of supersonic
velocity first appeared for the rear inlet location at 0.70 Mach number
(fig. 18), while supersonic velocity was not found at the forward inlet
location below 0.80 free-stream Mach number (reference 3). Earlier and
more intense shock waves at the rear locations and interaction of these
shock waves with the boundary layer at the rear inlet locations caused
losses in ram recovery greater than those at the more forward locations.
The critical pressure coefficients shown in the pressure-distribution
figures were calculated for isentropic flow. Hence, for points where the
total pressure was less than the free-stream total pressure (such as
behind the lip leading edge), the critical pressure coefficients are some-
what in error. Likewise, the velocities inside the duct are not exactly
as would be computed from the pressure coefficients by the isentropic
relations.

A further effect of the wing-induced velocity was curvature of the
flow, evidenced in the tuft pictures in reference 3, that resulted in an
upflow along the fuselage adjacent to the wing leading edge and a downflow
farther aft along the fuselage. The curved flow introduced a component
of velocity perpendicular to the inlet center line. This perpendicular
component probably interfered with the flow down the ramp and contributed
to the ram-recovery losses at the rear inlets.

The areas of low ram recovery at the outer corners of the rearmost
inlet, shown in figures 10(n), 10(o), and 10(s) and stated earlier as
having been due in part to boundary layer, are thought to have been due
also to shock waves. The pressure plots of figures 18 through 24 (for
the rear inlet) indicate that shock waves were always of greater inten-
sity along the lower ramp wall and usually of greater intensity along
the upper ramp wall than along the ramp center. Interaction of these
stronger shock waves along the ramp walls with the boundary layer probably
contributed to the losses in the outer corners of the inlet. Contours of
ram-recovery ratio for the most forward inlet (reference 3) showed no
evidence of losses in the outer corners of the inlet.

Effect of Angle of Attack

Ram-recovery ratio at the inlets in the two forward locations (fig. 9) generally decreased gradually with increasing angle of attack. This decrease in recovery was probably due to the increase in fuselage boundary-layer thickness with increasing angle of attack, as shown in reference 4. Ram-recovery ratio at the inlets in the two rear locations (fig. 9) decreased gradually with increasing angle of attack at Mach numbers below 0.70, but, at Mach numbers of 0.70 and higher, ram recovery decreased sharply, especially as the angle of attack increased above 0°. This sharp decline in ram recovery at the rear inlets with increasing angle of attack is thought to have been due to the increasing intensity of shock waves at the rear inlet locations with increasing angle of attack. This increase in shock-wave intensity is indicated by the increase in local supersonic velocities with increasing angle of attack in the pressure plots of figures 18 through 24. The most rearward inlet was probably further influenced by the shock waves from the wing. At the higher angles of attack, even the inlet in the third position might have been influenced by the shock waves from the wing.

CONCLUSIONS

Results of an investigation of NACA submerged inlets on a model of a hypothetical airplane indicate the following:

1. Mass-flow ratios between 0.60 and 0.80 are optimum for efficient operation of the inlets as indicated by pressure measurements 2.1 inches behind the lip leading edge. Within this range, ram-recovery ratios of 0.94 for the forward inlet and 0.90 for the rear inlet were measured.

2. Inlets in the region of high-velocity flow induced by the wing had high compressibility losses beginning at approximately 0.70 Mach number, while those ahead of this region maintained high ram recovery at the highest test Mach number.

Ames Aeronautical Laboratory,
    National Advisory Committee for Aeronautics,
        Moffett Field, Calif.

REFERENCES

1. Frick, Charles W., Davis, Wallace F., Randall, Lauros M., and Mossman, Emmet A.: An Experimental Investigation of NACA Submerged-Duct Entrances. NACA ACR 5I20, 1945.

2. Mossman, Emmet A., and Randall, Lauros M.: An Experimental Investigation of the Design Variables for NACA Submerged Duct Entrances. NACA RM A7I30, 1948.

3. Hall, Charles F., and Barclay, F. Dorn: An Experimental Investigation of NACA Submerged Inlets at High Subsonic Speeds. I – Inlets Forward of the Wing Leading Edge. NACA RM A8B16, 1948.

4. Hall, Charles F., and Frank, Joseph L.: Ram-Recovery Characteristics of NACA Submerged Inlets at High Subsonic Speeds. NACA RM A8I29, 1948.

5. Herriot, John G.: Blockage Corrections for Three-Dimensional-Flow Closed-Throat Wind Tunnels, With Consideration of the Effect of Compressibility. NACA RM A7B28, 1947.
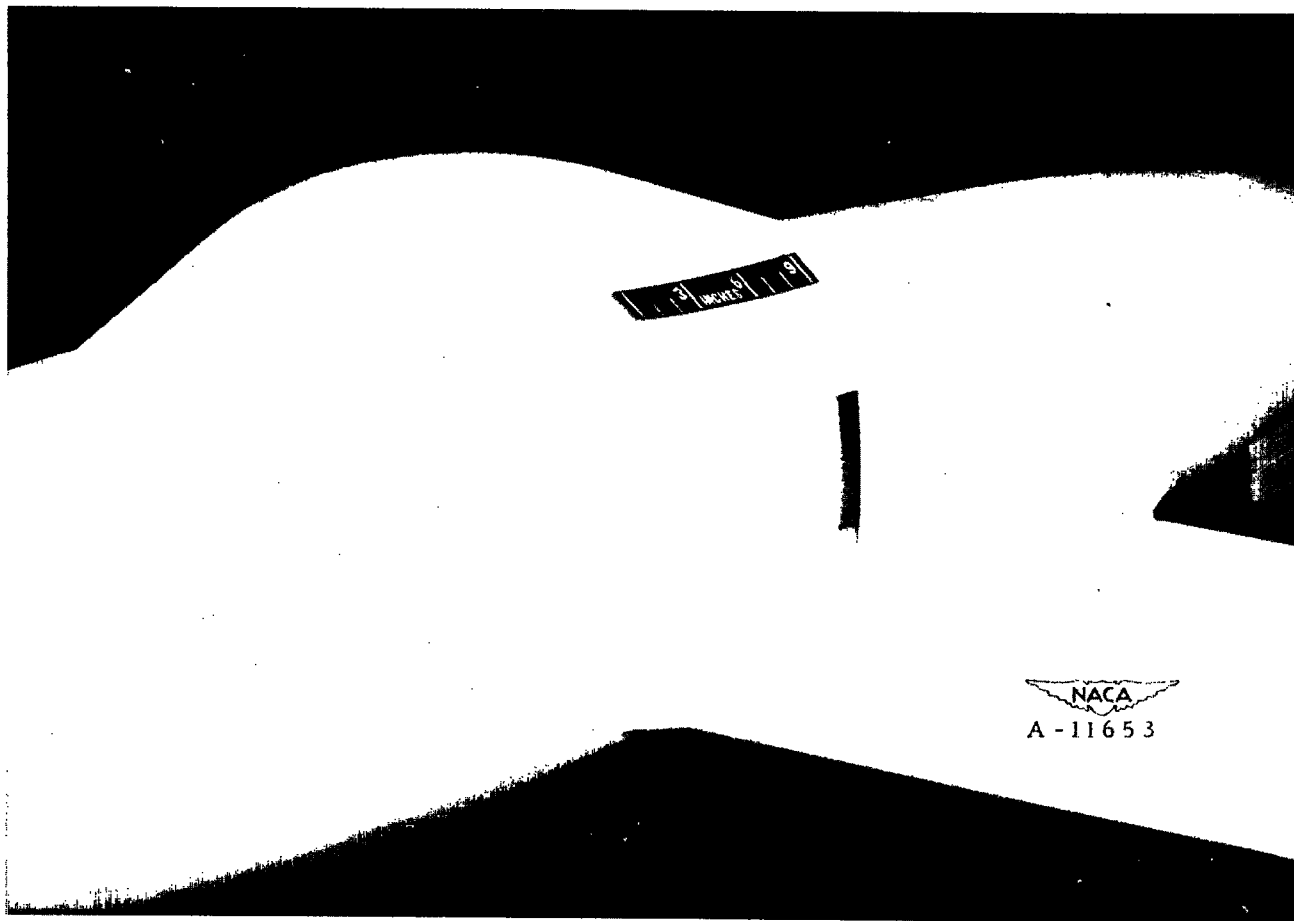
Figure 1.— Model with inlet at fuselage station 50.75.

Note:
Dimensions and stations are in inches unless otherwise noted.

25% wing chord

Inlet
Entrance area, (one) 0.0711 sq ft
Width   6.40 in.
Depth   1.60 in.

Wing
Section 63_1-110
Incidence   0°
Area   20.93 sq ft
Root chord   33.00 in.
Tip chord   16.50 in.
Mean aerodynamic chord
                     25.68 in.

¢

122.4

48

118

3.2

3.2

¢

Wing root chord is 7.2 inches below fuselage ¢

NACA

Fuselage sta.   34.25   50.75
              42.50   59.00
Inlet locations

Figure 2.—Submerged-inlet model.

Sec. AA
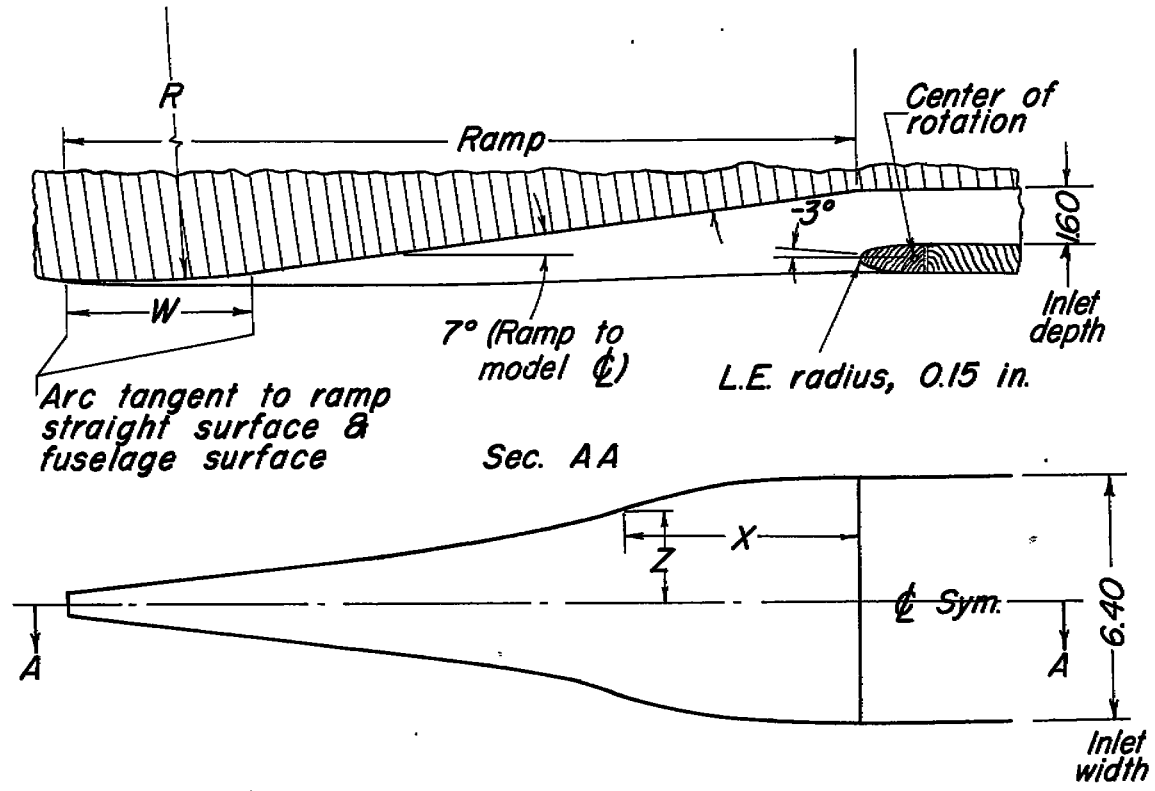
Lip coordinates
for −3° lip angle

Station	Outer Surface	Inner Surface
Inches from nose	Inches from fuselage surface	Inches from fuselage surface
0	0.372	0.372
.2	.193	.568
.4	.131	.638
.6	.085	.691
.8	.055	.725
1.0	.032	.747
1.2	.015	.759
1.4	.004	.761
1.6	0	.762
1.8	0	.762

Ramp-wall coordinates

X−(in.)	Z−(in.)
0	3.20
2.11	3.18
4.22	2.93
6.33	2.45
8.44	1.94
10.55	1.55
12.66	1.25
14.77	.99
16.88	.75
18.99	.51
21.10	.27

Ramp coordinates			
No.	Inlet location	W−(in.)	R−(in.)
1	34.25	8.60	32.40
2	42.50	5.02	29.70
3	50.75	3.75	28.85
4	59.00	3.75	30.70

Figure 3.−Dimensions of inlets.
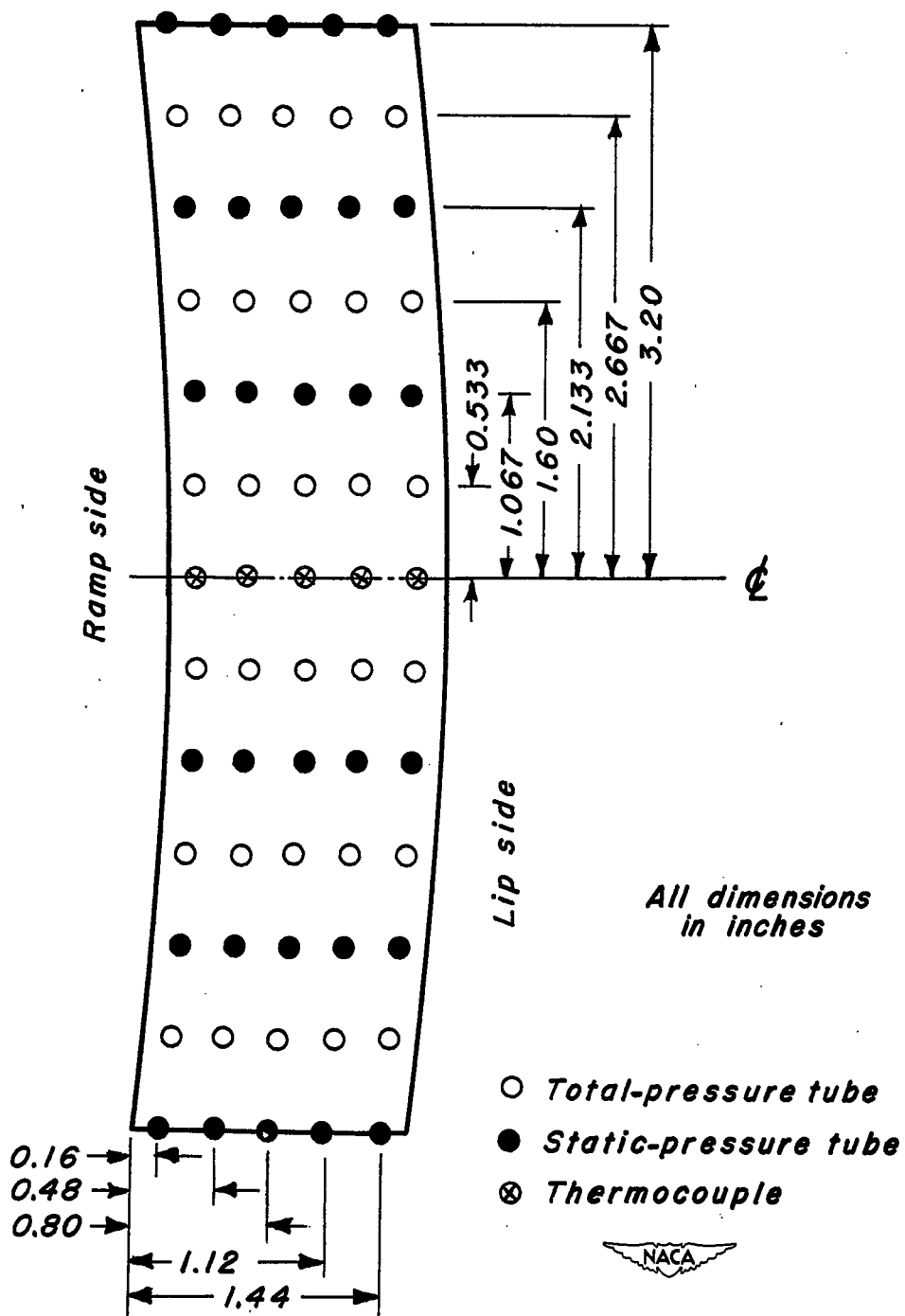
Figure 4.-Location of pressure tubes on rake 2.1 inches behind lip leading edge.
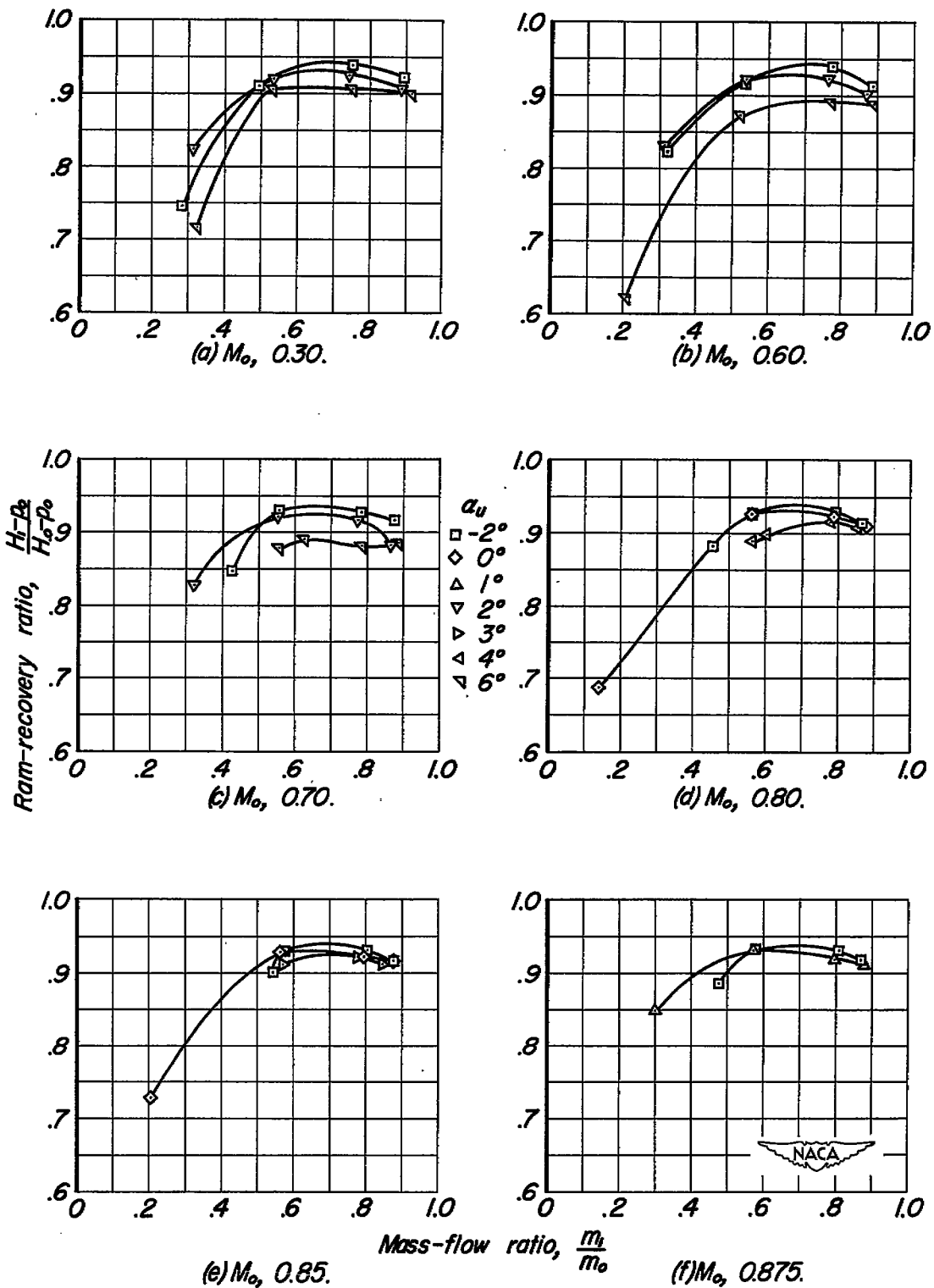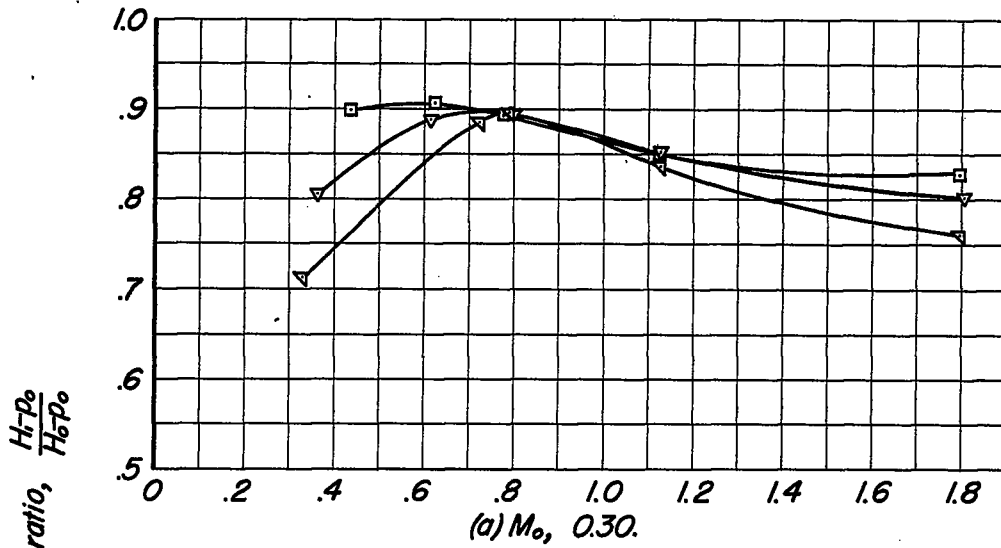
Figure 5.–Variation of ram-recovery ratio with mass-flow ratio for several angles of attack and Mach numbers. Inlets at fuselage station 34.25.

(a) M_o, 0.30.

(b) M_o, 0.60.

Mass-flow ratio, $\frac{m_i}{m_o}$

Ram-recovery ratio, $\frac{H_i - p_o}{H_o - p_o}$

α_u
□ -2°
▽ 2°
◁ 6°
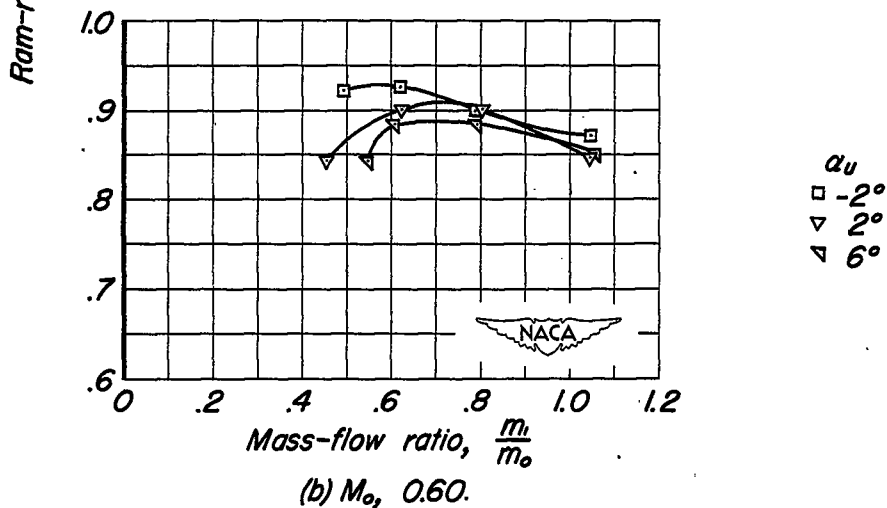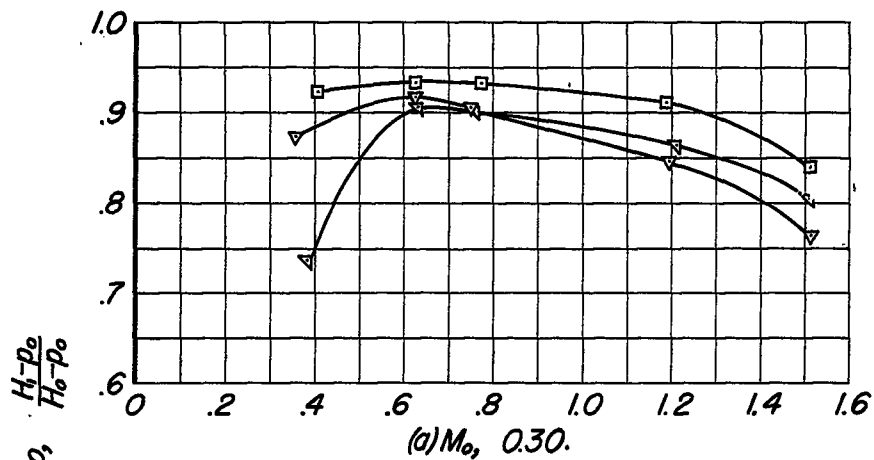
Figure 6.—Variation of ram-recovery ratio with mass-flow ratio for several angles of attack and Mach numbers. Inlets at fuselage station 42.50.

(c) M₀, 0.70.

(d) M₀, 0.80.

(e) M₀, 0.85.

Mass-flow ratio, $\frac{m_i}{m_o}$

(f) M₀, 0.875.

a_u
□ -2°
◇ 0°
△ 1°
▽ 2°
▷ 3°
◁ 4°
◁ 6°

Ram-recovery ratio, $\frac{H-p_o}{H_o-p_o}$
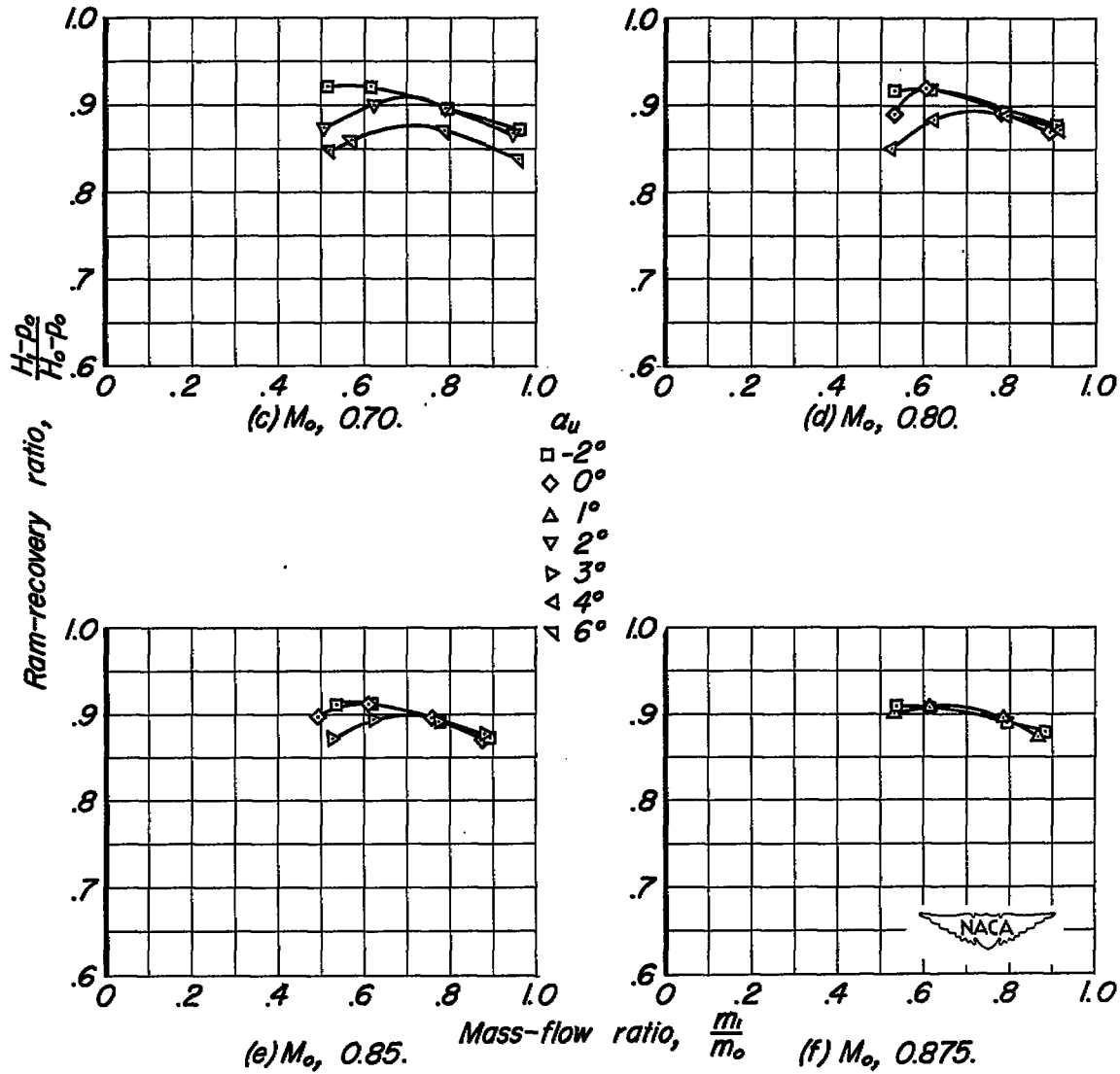
Figure 6.—Concluded.

(a) M_o, 0.30.

(b) M_o, 0.60.

a_u
□ -2°
▽ 2°
◁ 6°
▷ 9°
△ 12°
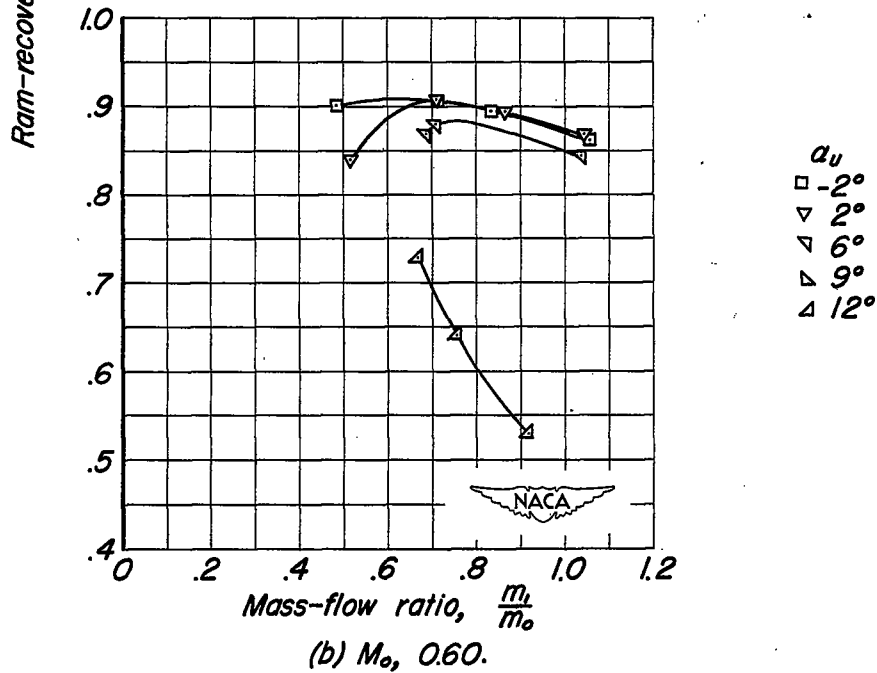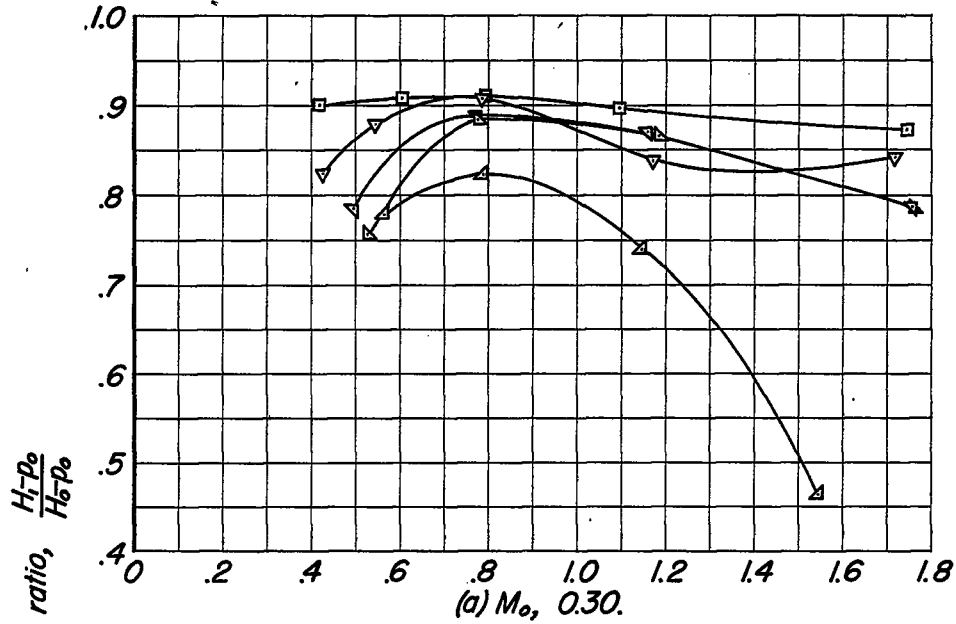
Figure 7.—Variation of ram-recovery ratio with mass-
flow ratio for several angles of attack and Mach
numbers. Inlets at fuselage station 50.75.

α_u
□ -2°
◇ 0°
△ 1°
▽ 2°
▷ 3°
◁ 4°
▽ 6°

(c) M_o, 0.70.

(d) M_o, 0.80.

(e) M_o, 0.85.

(f) M_o, 0.875.

Ram-recovery ratio, $\dfrac{H_i - p_o}{H_o - p_o}$

Mass-flow ratio, $\dfrac{m_i}{m_o}$

Figure 7.— Concluded.

(a) M_o, 0.30.

(b) M_o, 0.60.

a_u
□ -2°
▽ 2°
◁ 6°

Ram-recovery ratio, $\frac{H_i - p_o}{H_o - p_o}$
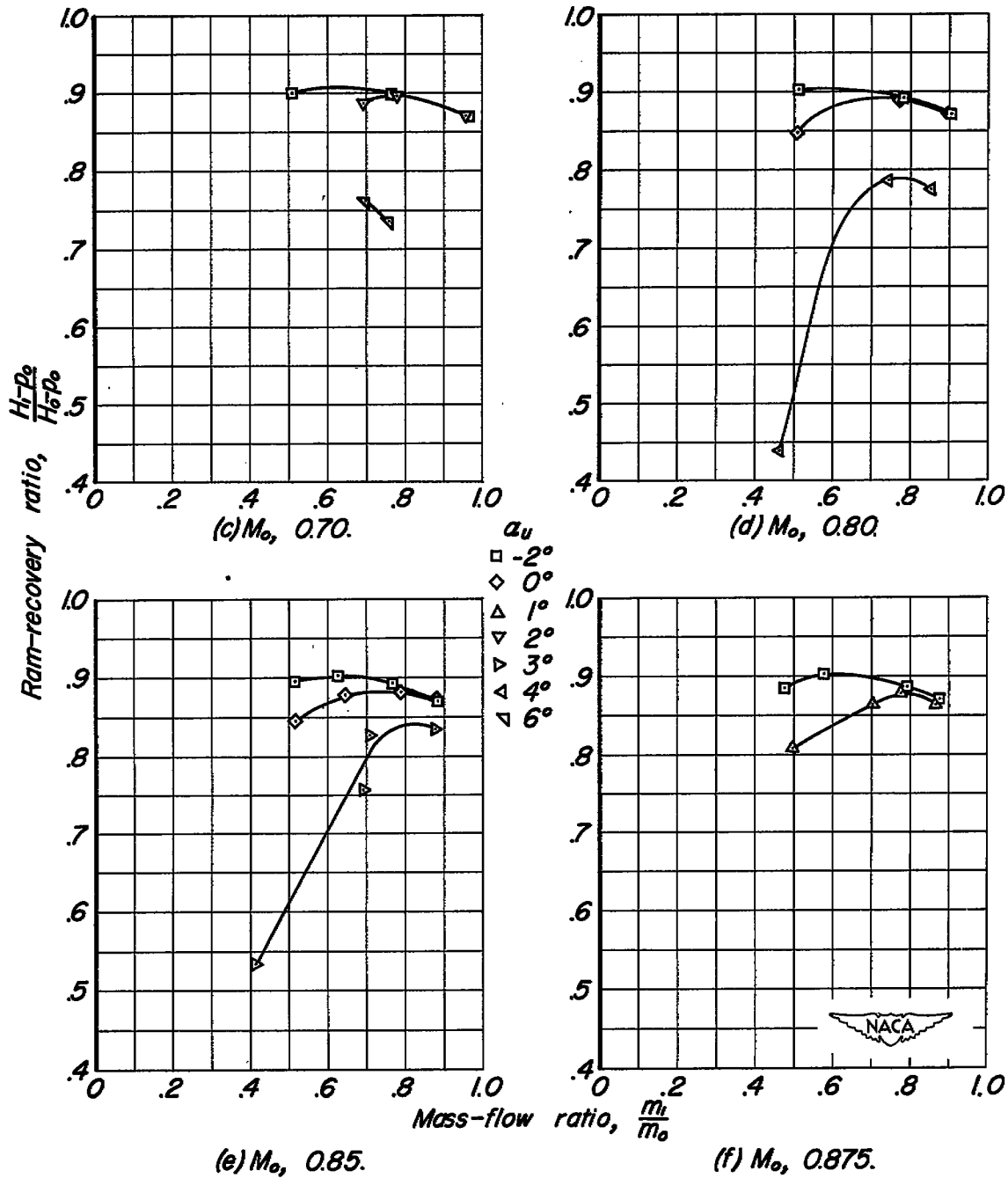
Mass-flow ratio, $\frac{m_i}{m_o}$
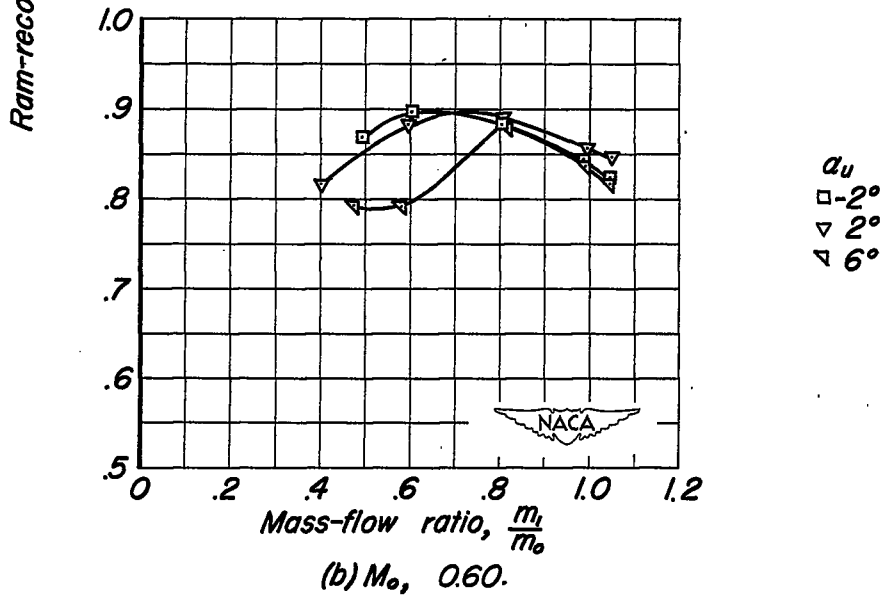
Figure 8.-Variation of ram-recovery ratio with mass-flow ratio for several angles of attack and Mach numbers. Inlets at fuselage station 59.00.
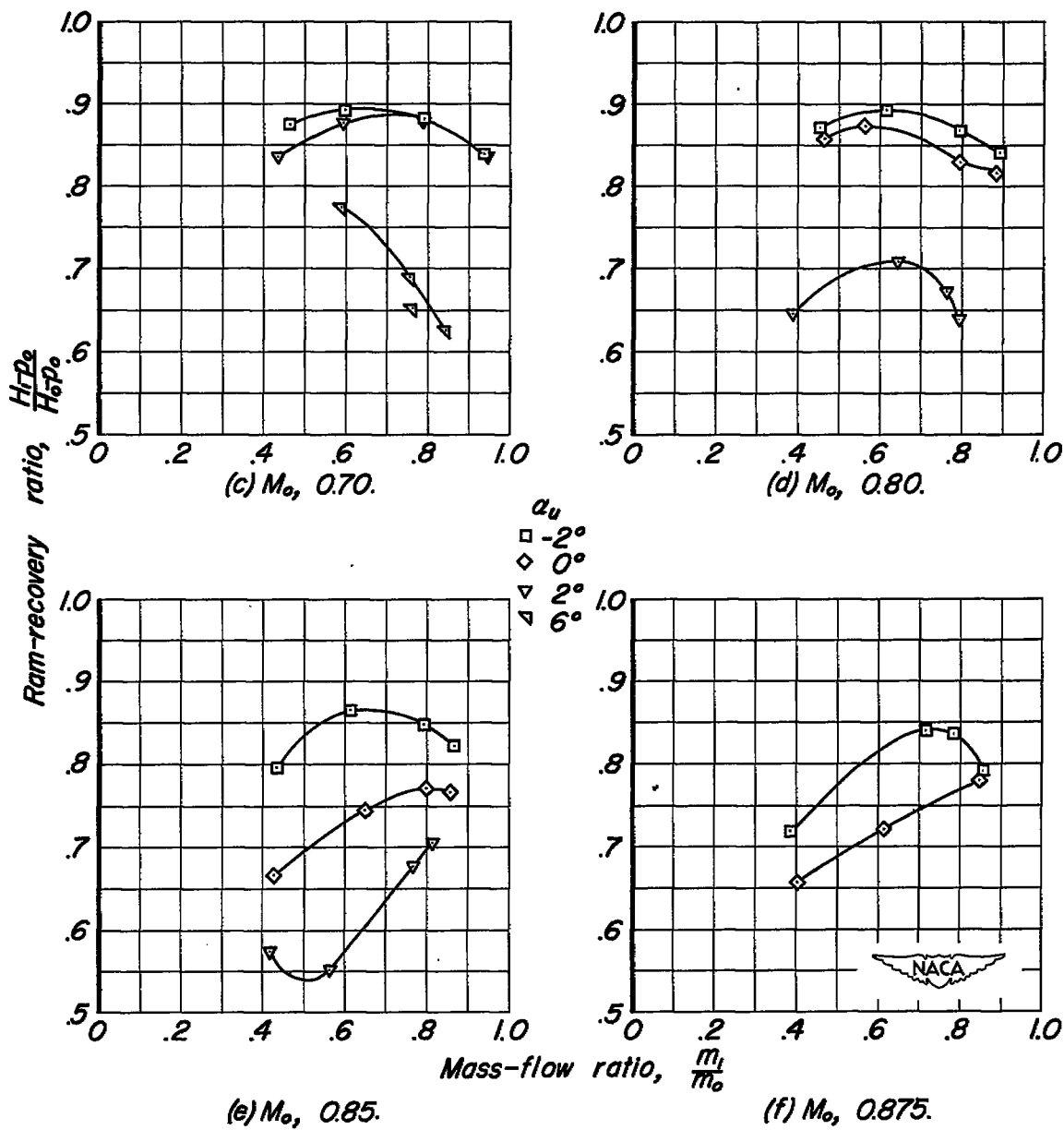
CONFIDENTIAL

Figure 8.-Concluded.

CONFIDENTIAL

(a) $\frac{m_i}{m_o}$, 0.60.
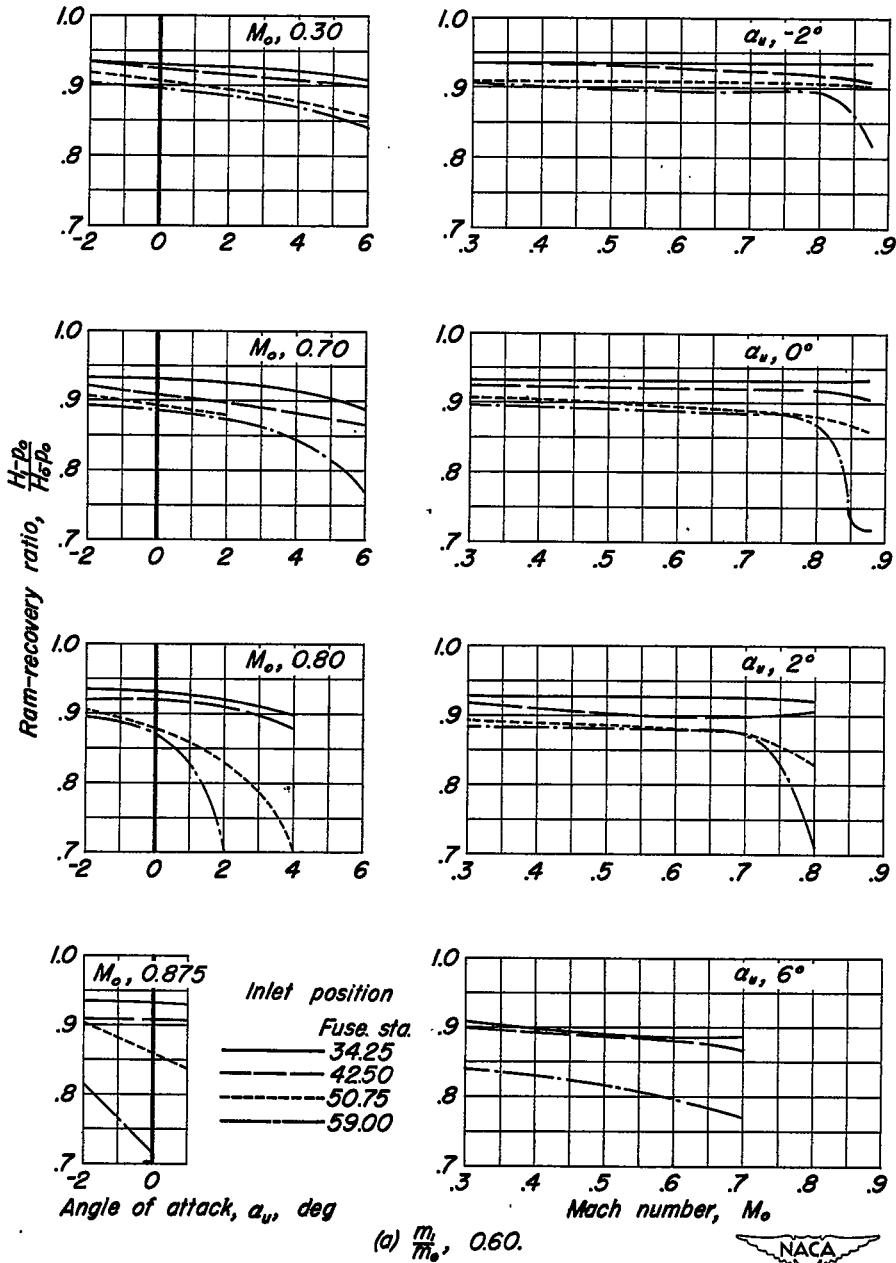
Figure 9.—Effect of inlet location on ram-recovery ratio with varying angle of attack and Mach number.

Inlet position

Fuse. sta.
————— 34.25
————— 42.50
----- 50.75
—·—·— 59.00

Angle of attack, a_u , deg

Mach number, M_o

(b) $\frac{m_i}{m_o}$, 0.80.

NACA

Figure 9.—Concluded.

NACA RM A50E02

23

Ram-recovery ratio

Ramp side

Mass-flow ratio

Lip side

(a) M_o, .30
α_u, -2°
$\frac{m_l}{m_o}$, .434
$\frac{H_l-p_o}{H_o-p_o}$, .897

(b) M_o, .80
α_u, -2°
$\frac{m_l}{m_o}$, .451
$\frac{H_l-p_o}{H_o-p_o}$, .872

(c) M_o, .875
α_u, -2°
$\frac{m_l}{m_o}$, .386
$\frac{H_l-p_o}{H_o-p_o}$, .719

(d) M_o, .30
α_u, -2°
$\frac{m_l}{m_o}$, .775
$\frac{H_l-p_o}{H_o-p_o}$, .893

(e) M_o, .80
α_u, -2°
$\frac{m_l}{m_o}$, .792
$\frac{H_l-p_o}{H_o-p_o}$, .868
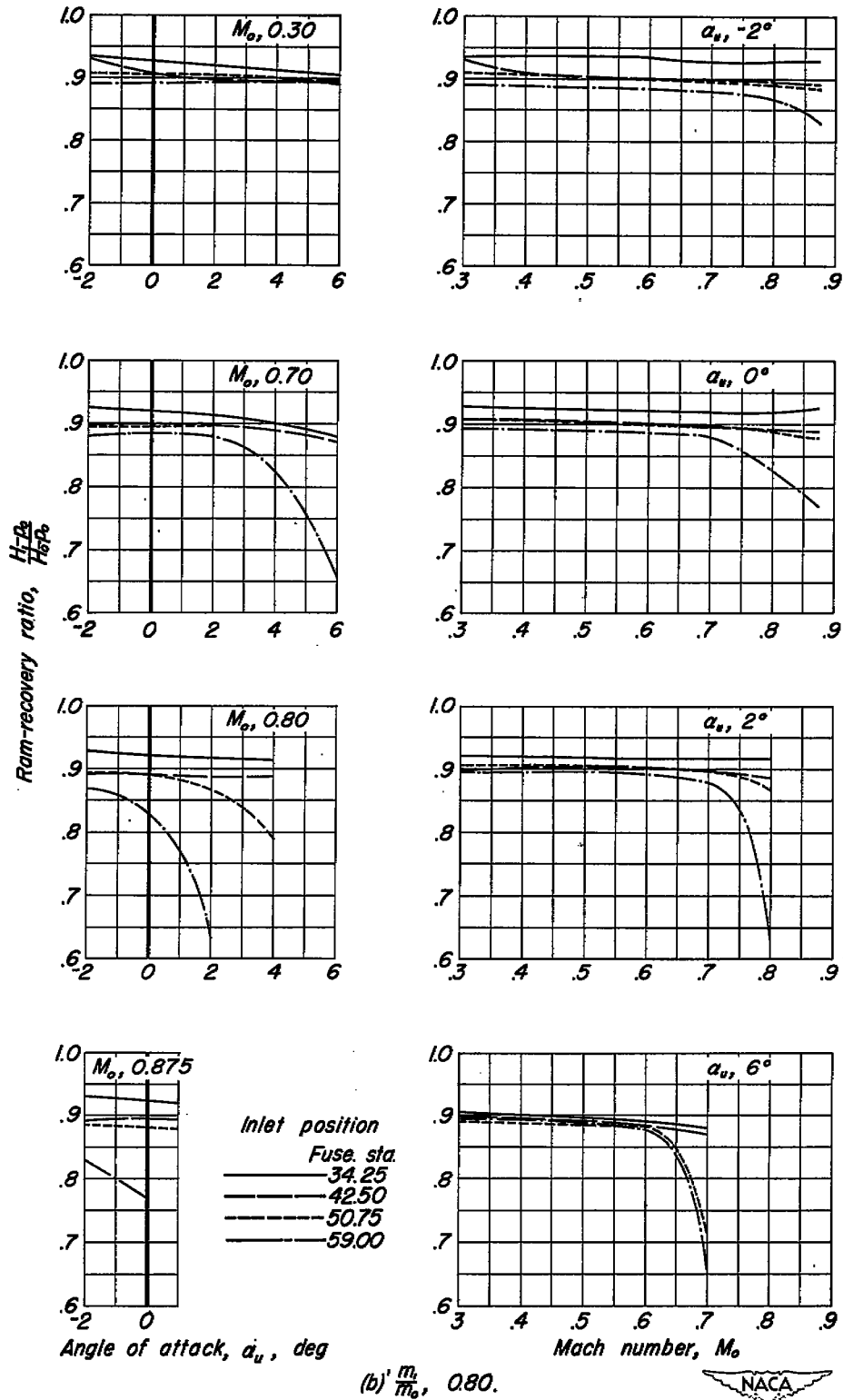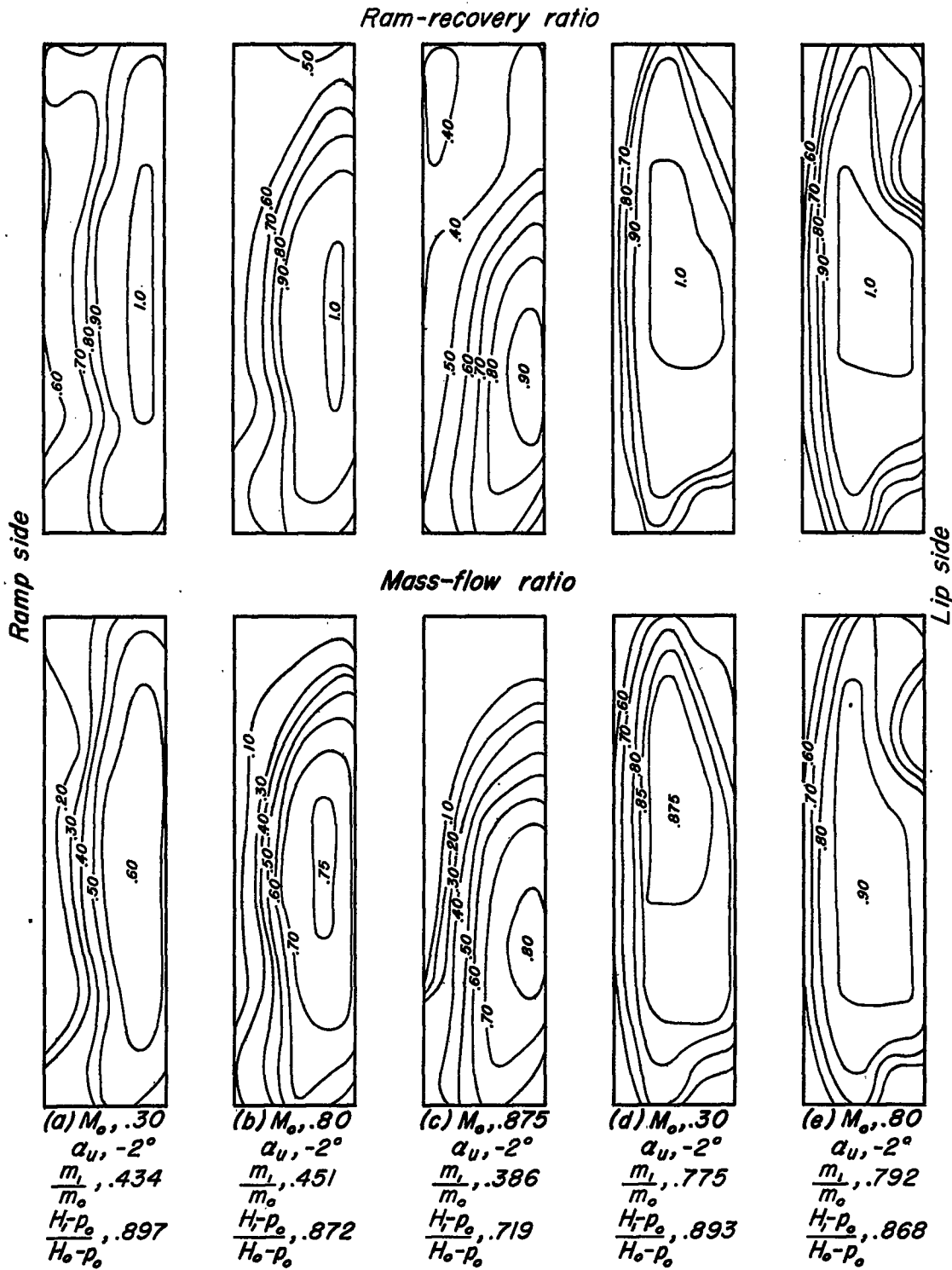
Figure 10.-Ram-recovery and mass-flow contours at inlet entrance. Inlet at station 59.00.

Ram-recovery ratio

Ramp side

Lip side
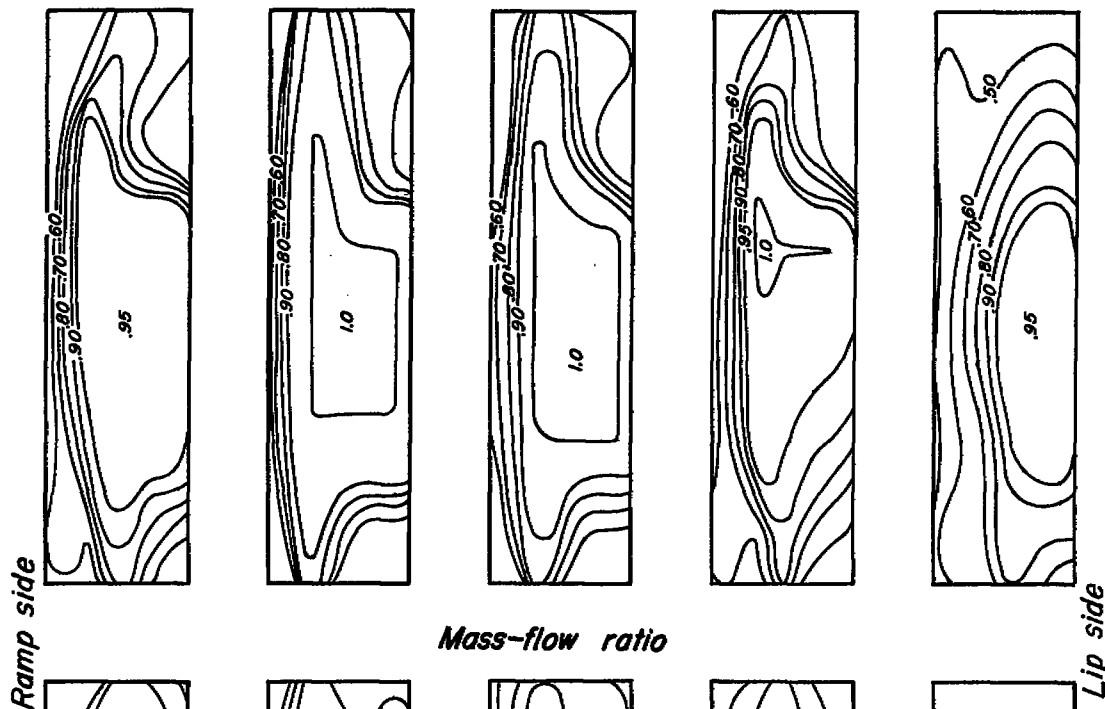
Mass-flow ratio

(f) M_o, .875
α_u, -2°
$\dfrac{m_I}{m_o}$, .785
$\dfrac{H_I-p_o}{H_o-p_o}$, .836

(g) M_o, .30
α_u, -2°
$\dfrac{m_I}{m_o}$, 1.126
$\dfrac{H_I-p_o}{H_o-p_o}$, .850

(h) M_o, .80
α_u, -2°
$\dfrac{m_I}{m_o}$, .891
$\dfrac{H_I-p_o}{H_o-p_o}$, .841

(i) M_o, .875
α_u, -2°
$\dfrac{m_I}{m_o}$, .854
$\dfrac{H_I-p_o}{H_o-p_o}$, .792

(j) M_o, .80
α_u, 0°
$\dfrac{m_I}{m_o}$, .463
$\dfrac{H_I-p_o}{H_o-p_o}$, .858
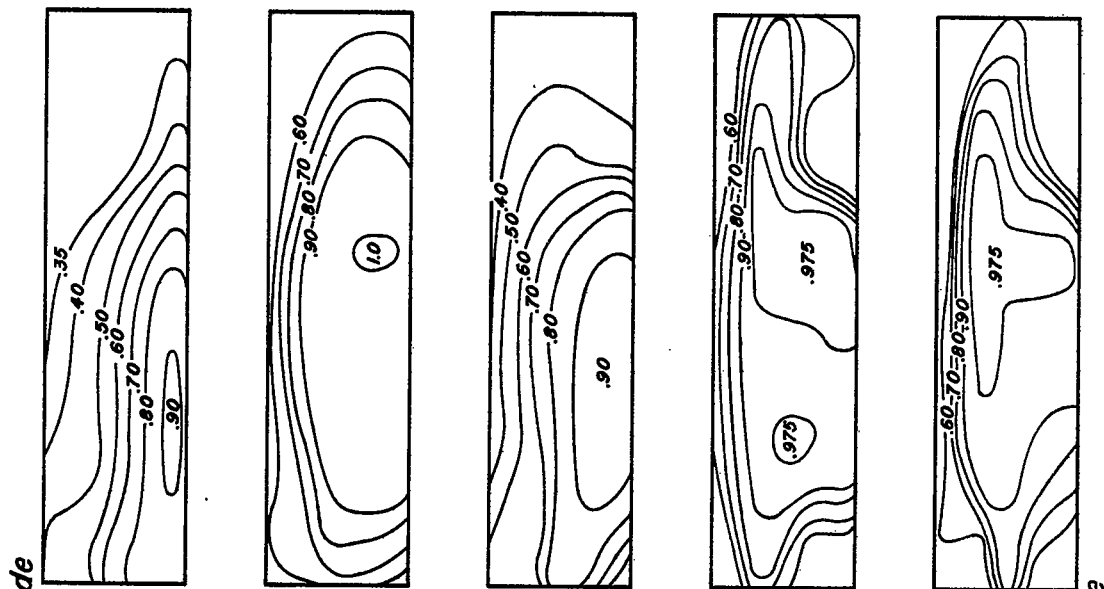
Figure 10.—Continued.

Figure 10.-Continued.

Ram-recovery ratio

Mass-flow ratio

Ramp side

Lip side

(p) M_o, .30
a_u, 2°
$\dfrac{m_l}{m_o}$, .361
$\dfrac{H_l-p_o}{H_o-p_o}$, .806

(q) M_o, .80
a_u, 2°
$\dfrac{m_l}{m_o}$, .391
$\dfrac{H_l-p_o}{H_o-p_o}$, .646

(r) M_o, .30
a_u, 2°
$\dfrac{m_l}{m_o}$, .614
$\dfrac{H_l-p_o}{H_o-p_o}$, .888

(s) M_o, .80
a_u, 2°
$\dfrac{m_l}{m_o}$, .644
$\dfrac{H_l-p_o}{H_o-p_o}$, .709

(t) M_o, .30
a_u, 2°
$\dfrac{m_l}{m_o}$, .799
$\dfrac{H_l-p_o}{H_o-p_o}$, .892

Figure 10.-Continued.

Ram-recovery ratio

Ramp side

Mass-flow ratio

Lip side

(u) M_o , .80
α_u , 2°
$\dfrac{m_i}{m_o}$, .794
$\dfrac{H_i-p_o}{H_o-p_o}$, .639

(v) M_o , .30
α_u , 6°
$\dfrac{m_i}{m_o}$, .329
$\dfrac{H_i-p_o}{H_o-p_o}$, .713

(w) M_o , .30
α_y , 6°
$\dfrac{m_i}{m_o}$, .725
$\dfrac{H_i-p_o}{H_o-p_o}$, .885

(x) M_o , .30
α_u , 6°
$\dfrac{m_i}{m_o}$, .785
$\dfrac{H_i-p_o}{H_o-p_o}$, .896
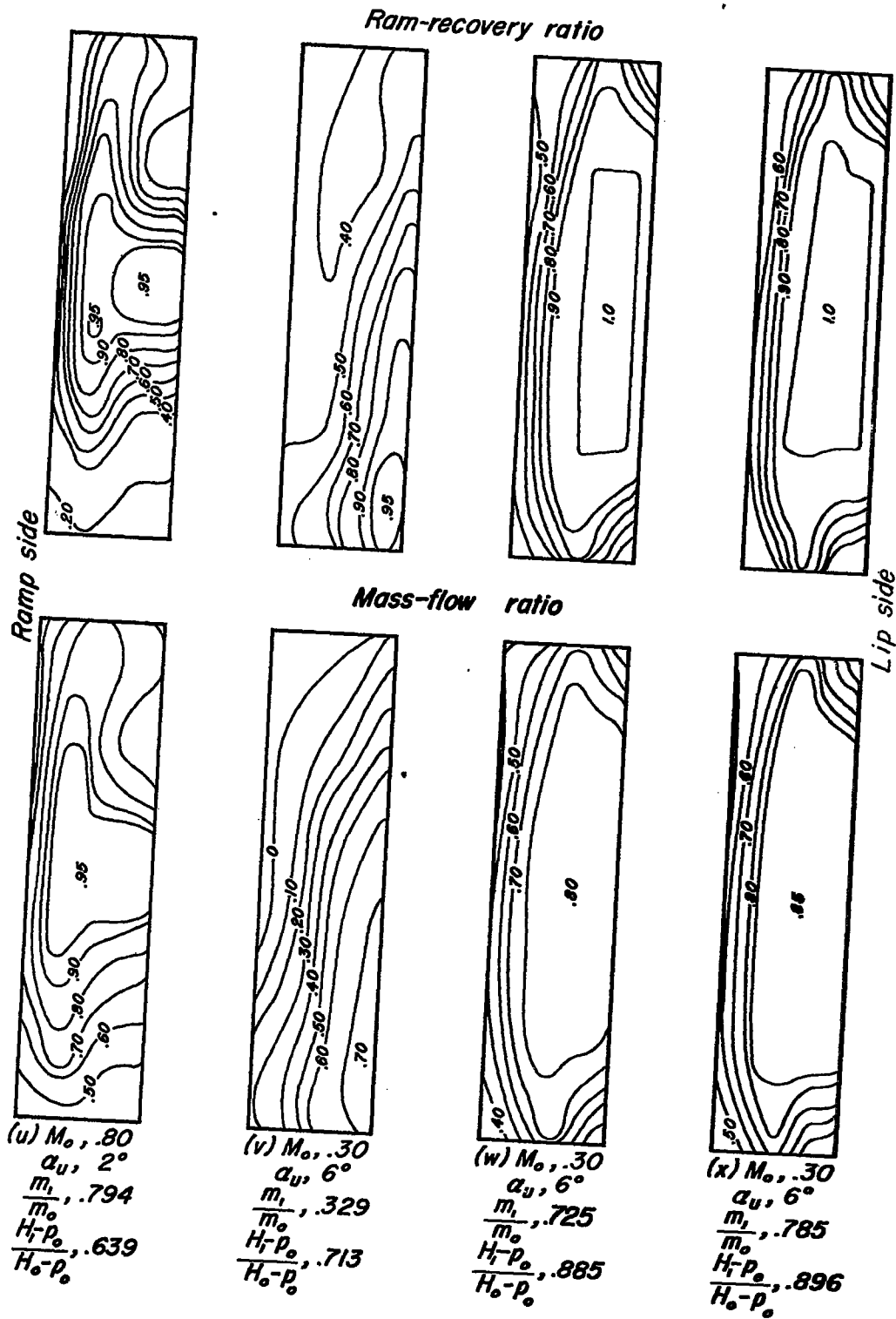
Figure   10.—Concluded.
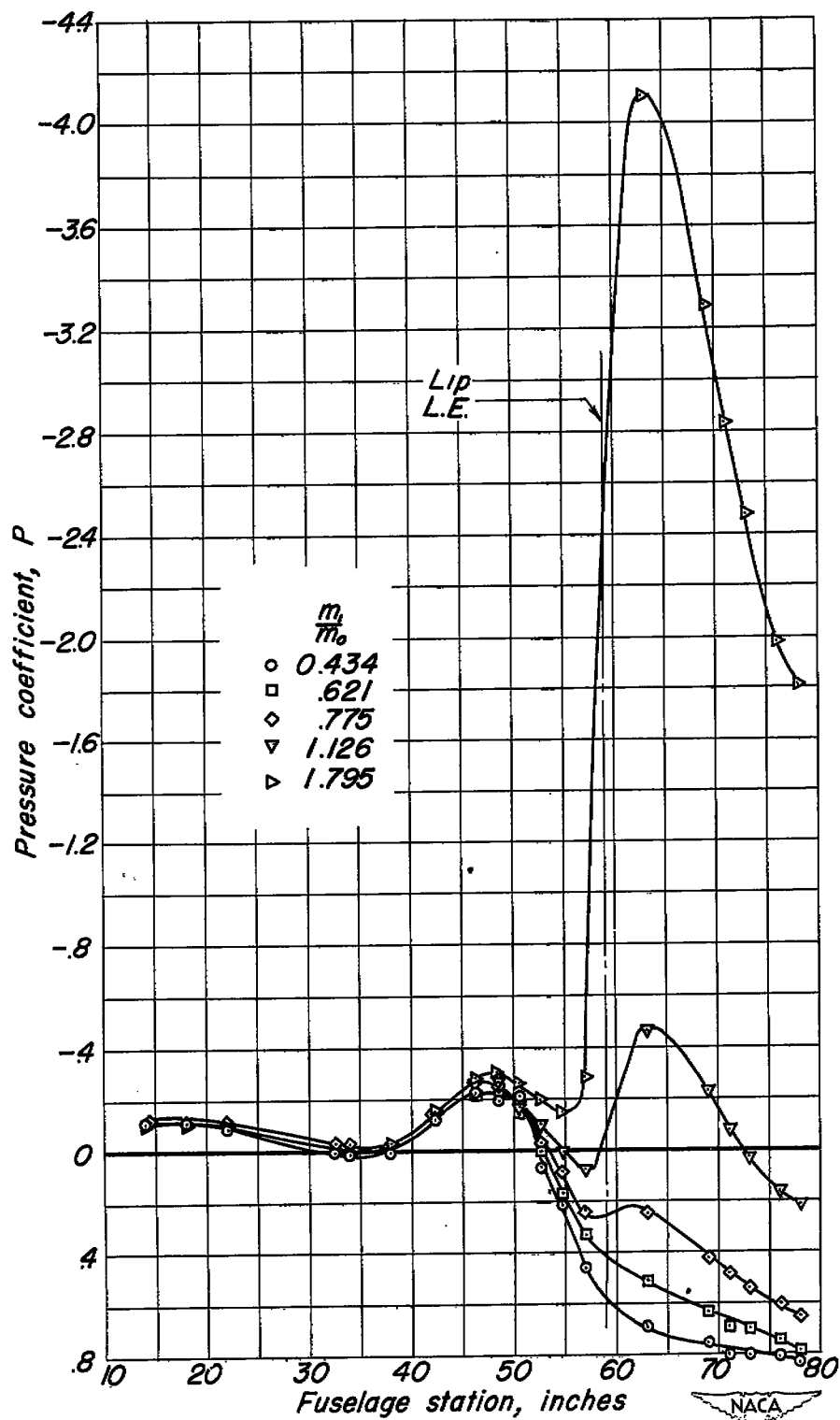
~~CONFIDENTIAL~~

Figure 11.—Pressure distribution along the ramp center line and inside the inlet. M_o, 0.30; α_u, -2°. Inlet at station 59.00.
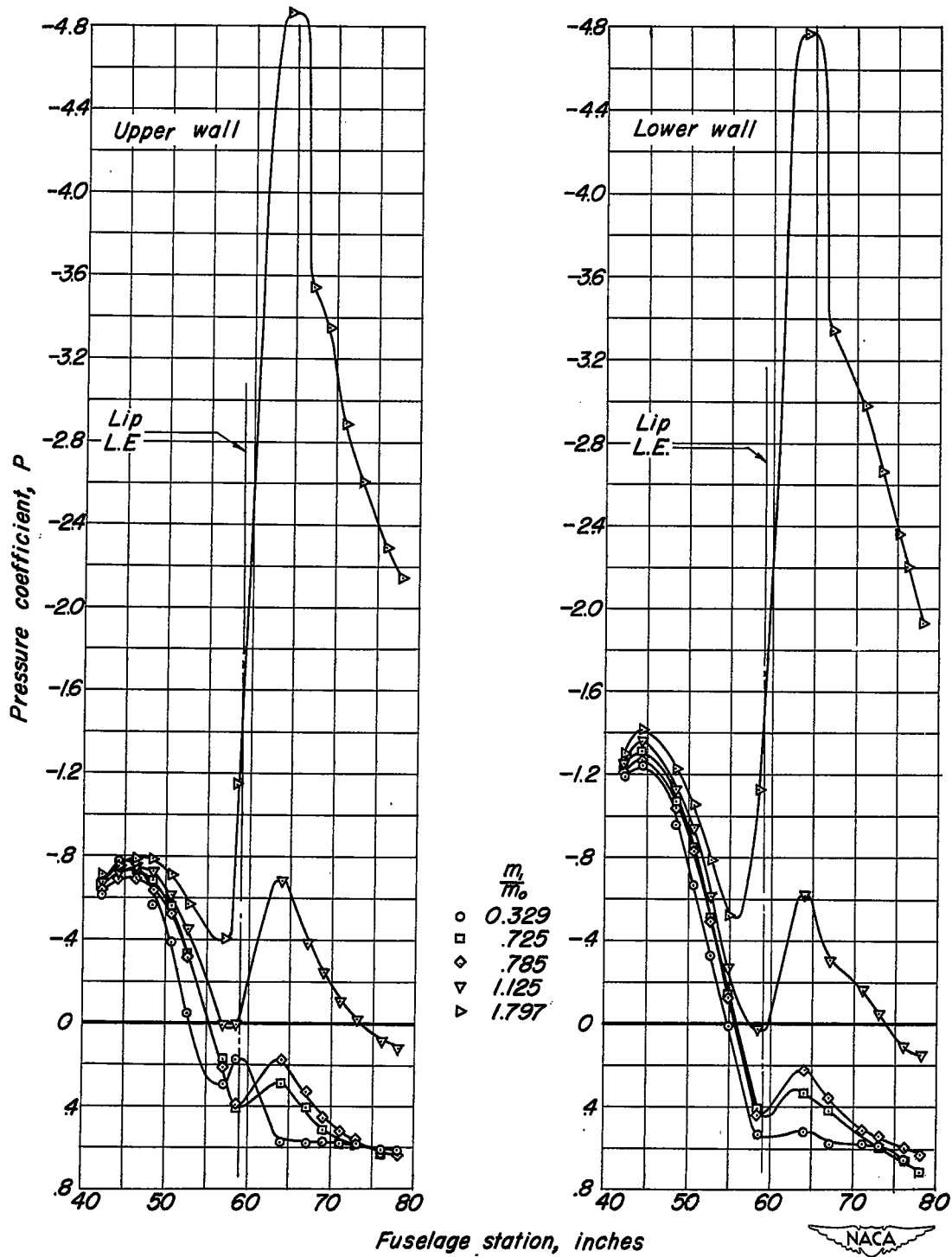
~~CONFIDENTIAL~~
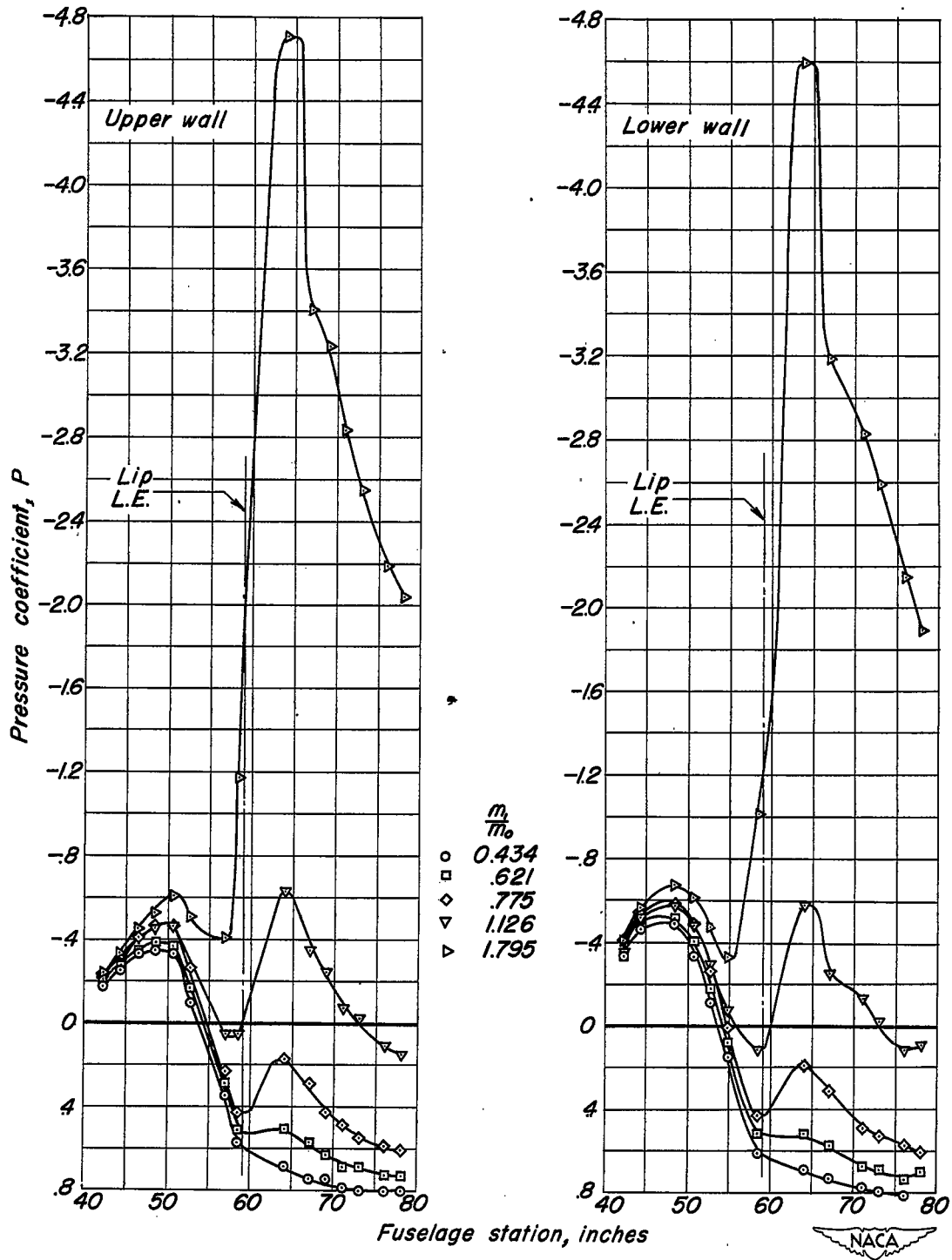
Figure 12.–Pressure distribution along the upper and lower walls of the ramp and inside the inlet. M_o, 0.30; α_u, −2°. Inlet at station 59.00.
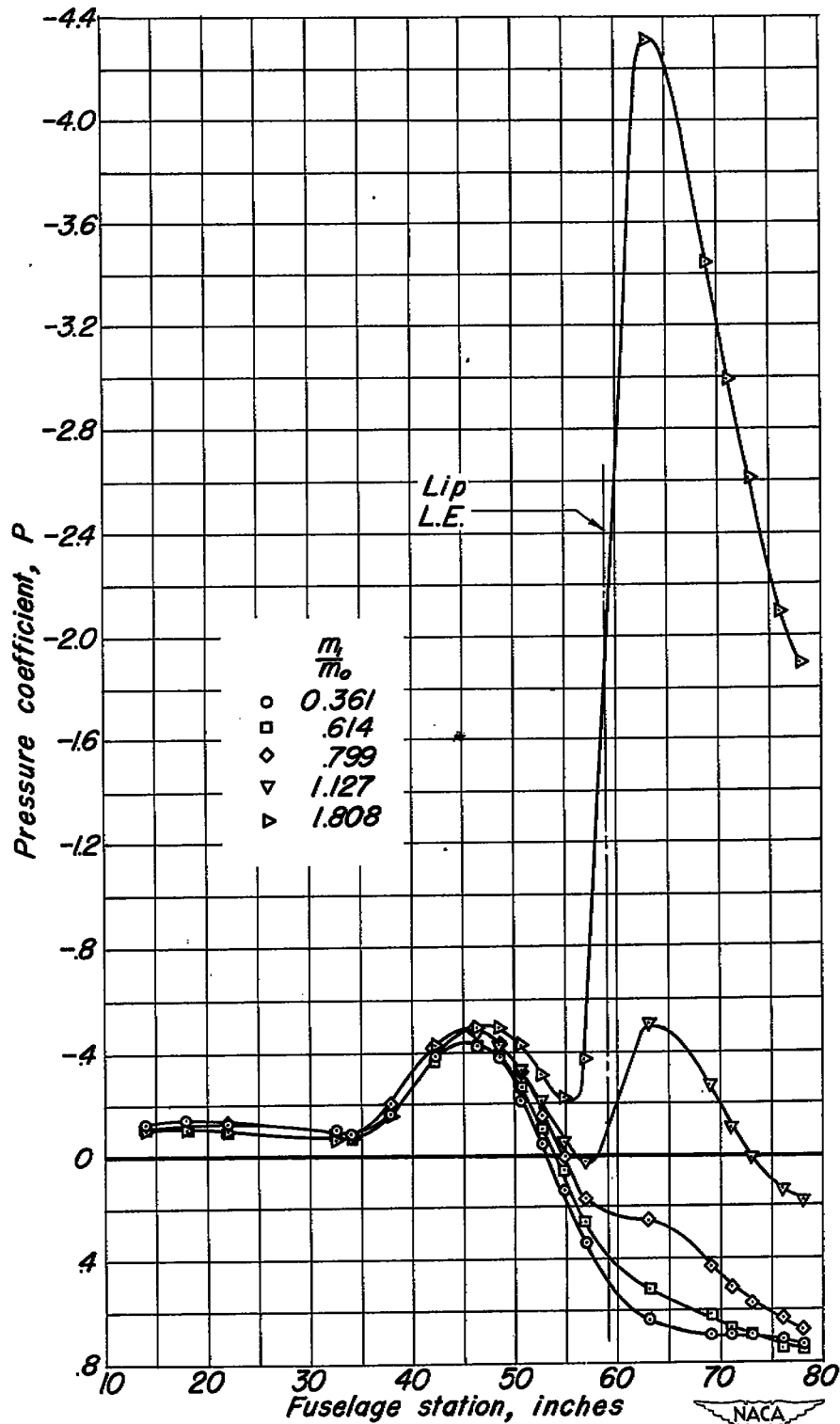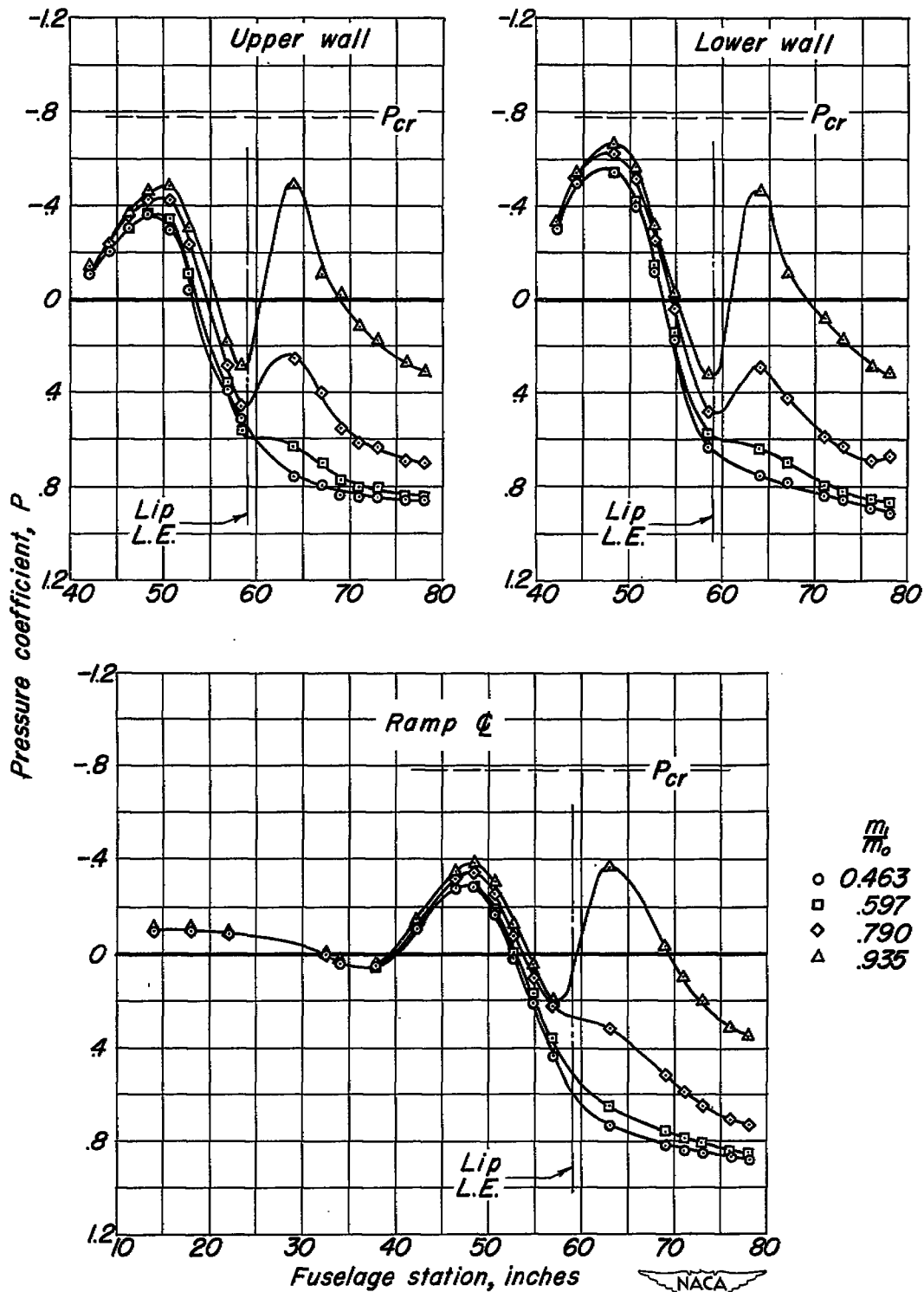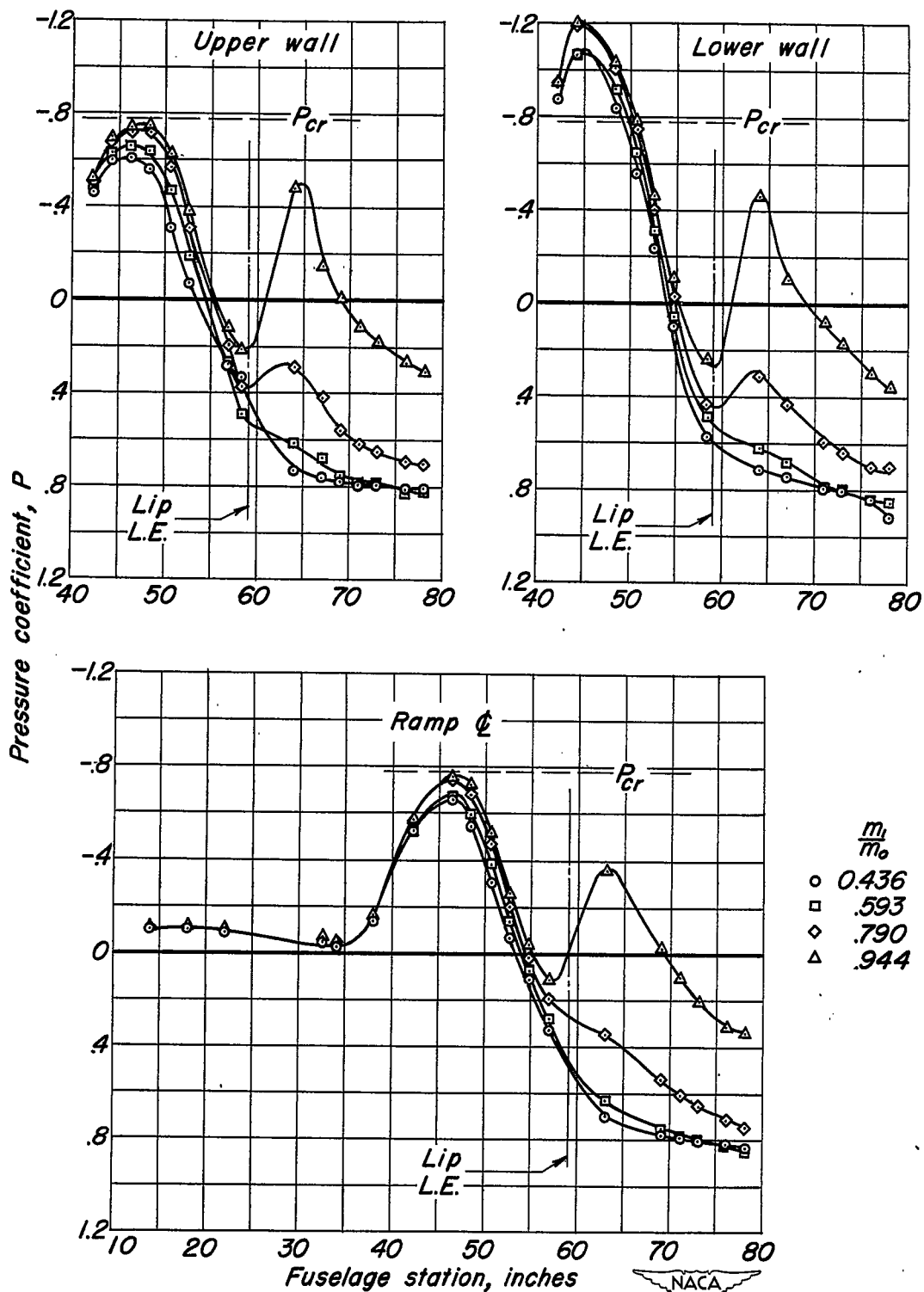
Figure 13.—Pressure distribution along the ramp center line and inside the inlet. M_o, 0.30; α_u, 2°. Inlet at station 59.00.
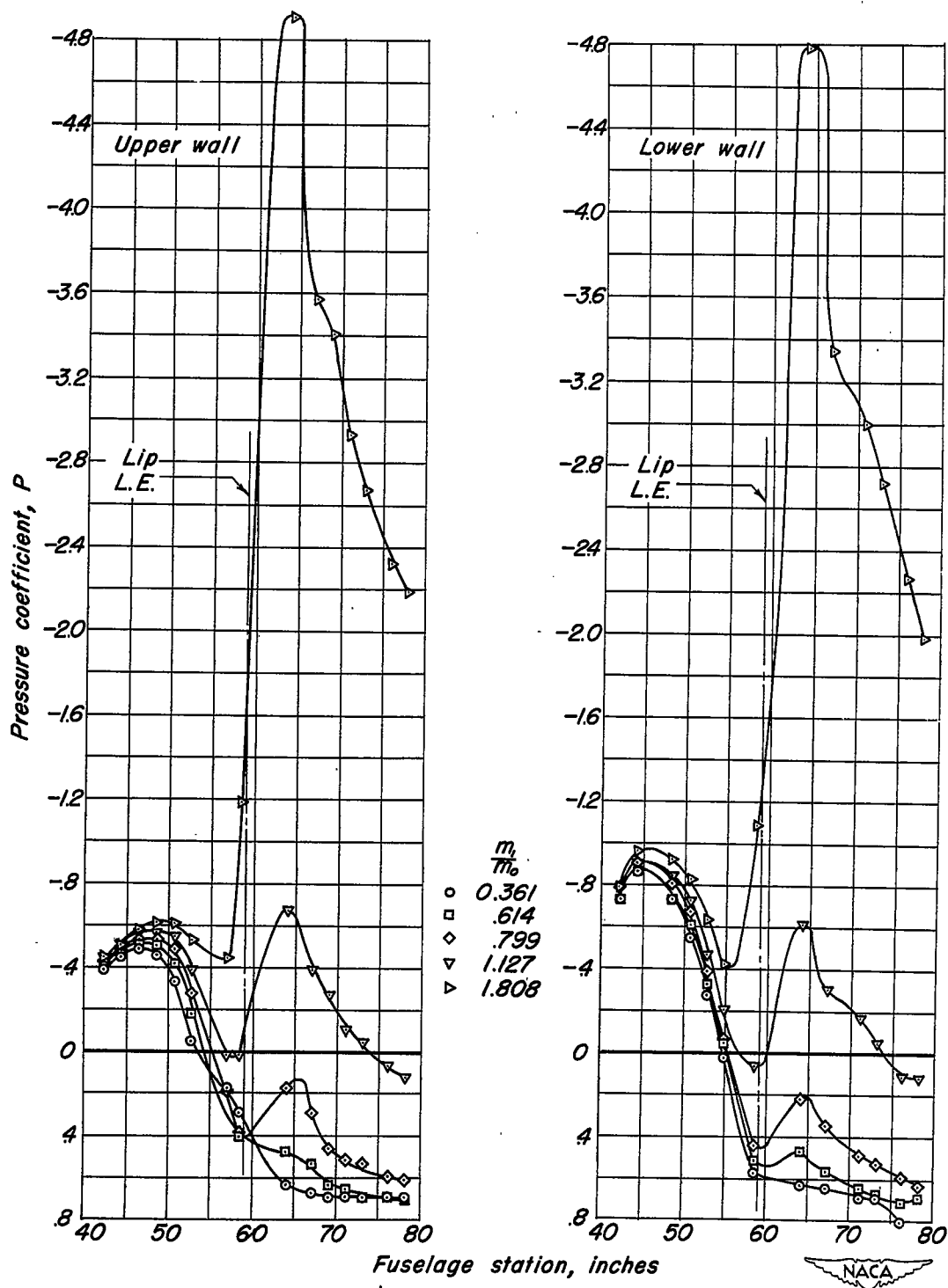
Figure 14.-Pressure distribution along the upper and lower walls of the ramp and inside the inlet. M_o, 0.30; α_u, 2°. Inlet at station 59.00.
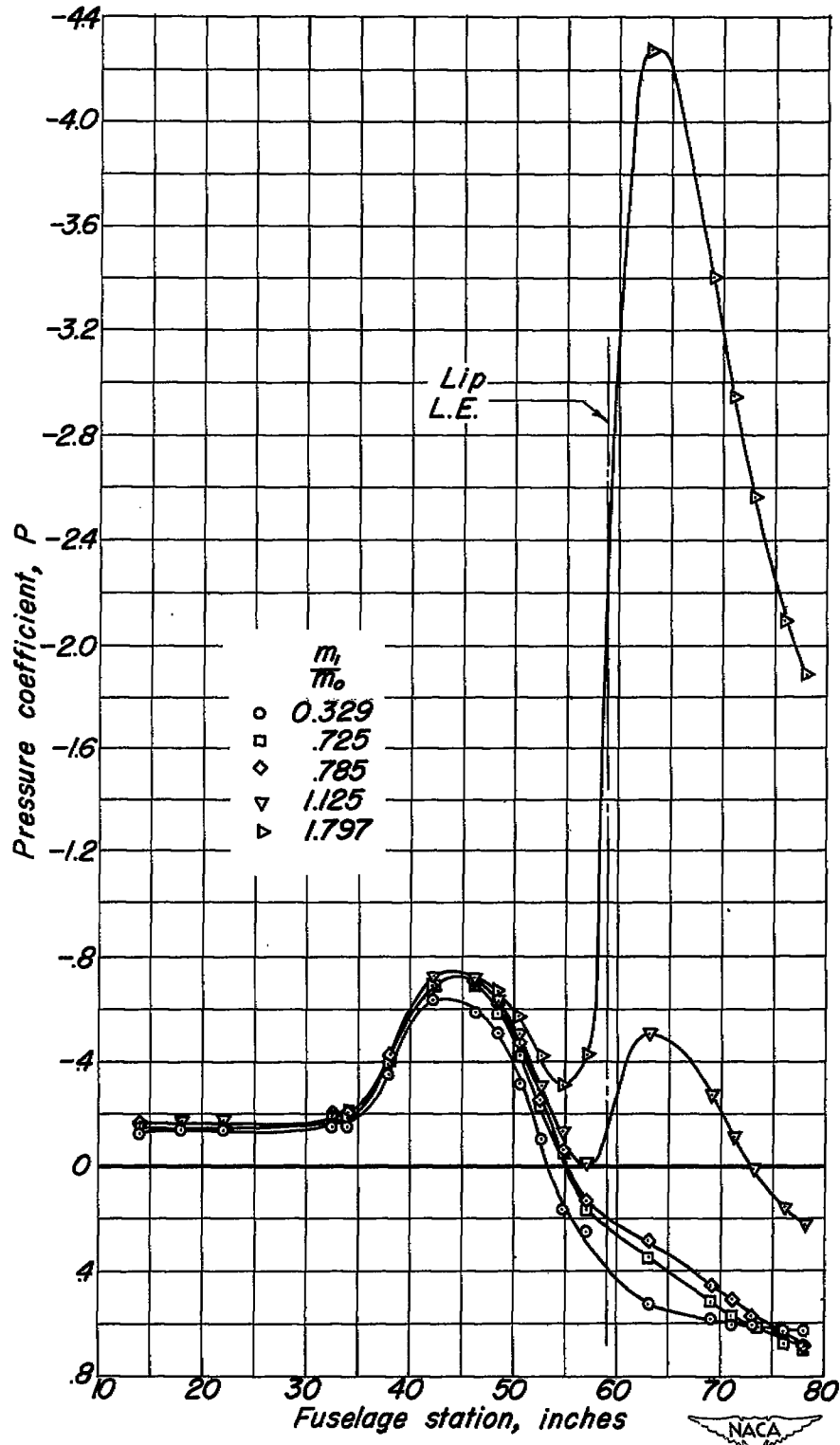
Figure 15.— Pressure distribution along the ramp center line and inside the inlet. M_o, 0.30; α_u, 6? Inlet at station 59.00.

~~CONFIDENTIAL~~

Figure 16.—Pressure distribution along the upper and lower walls of the ramp and inside the inlet. M_o, 0.30; α_u, 6°. Inlet at station 59.00.
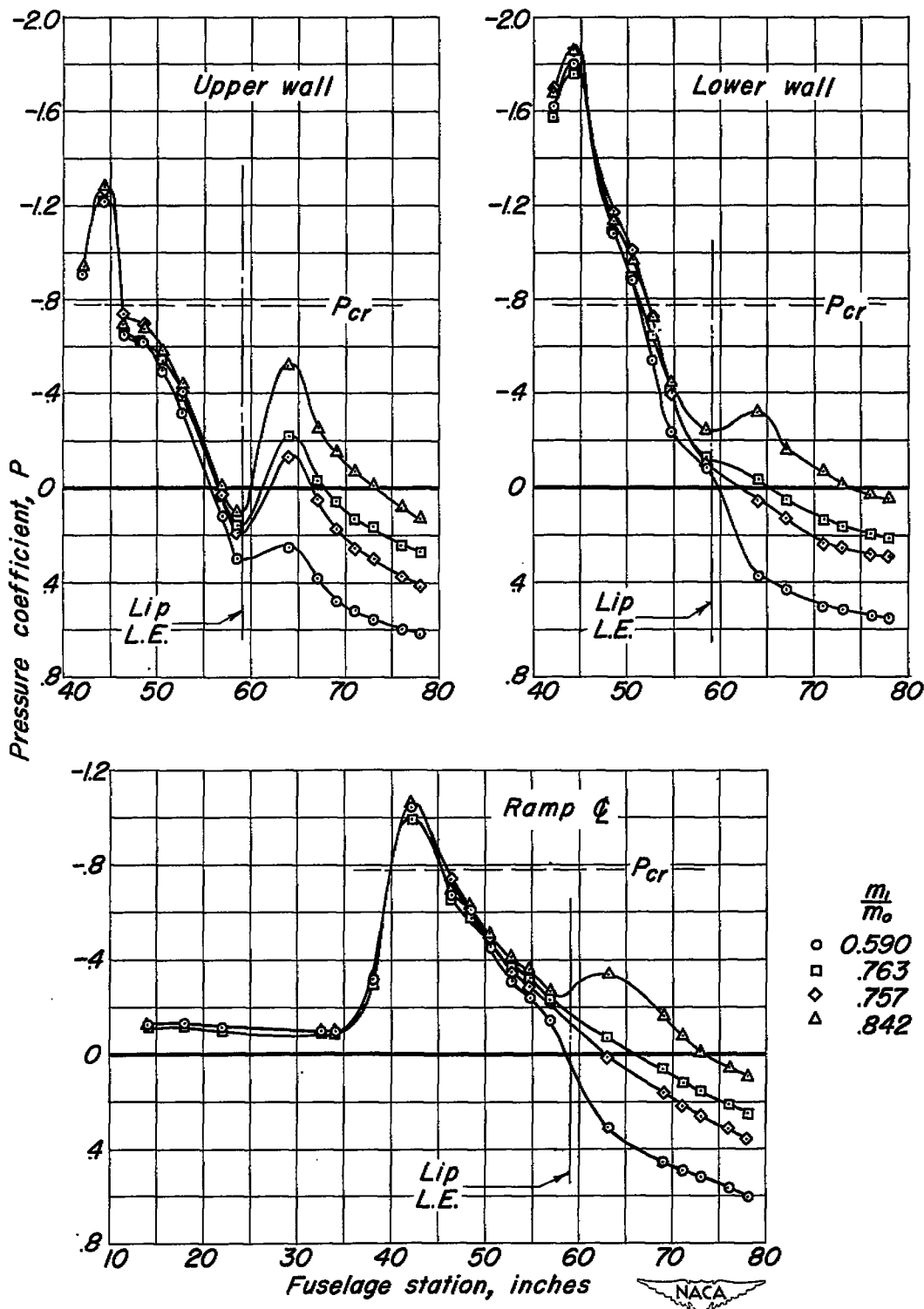
Figure 17.—Pressure distribution along the ramp center line, upper and lower walls of the ramp, and inside the inlet. M_o, 0.70; α_u, -2°. Inlet at station 59.00.

Figure 18.— Pressure distribution along the ramp center line, upper and lower walls of the ramp, and inside the inlet. M_o, 0.70; α_u, 2°. Inlet at station 59.00.
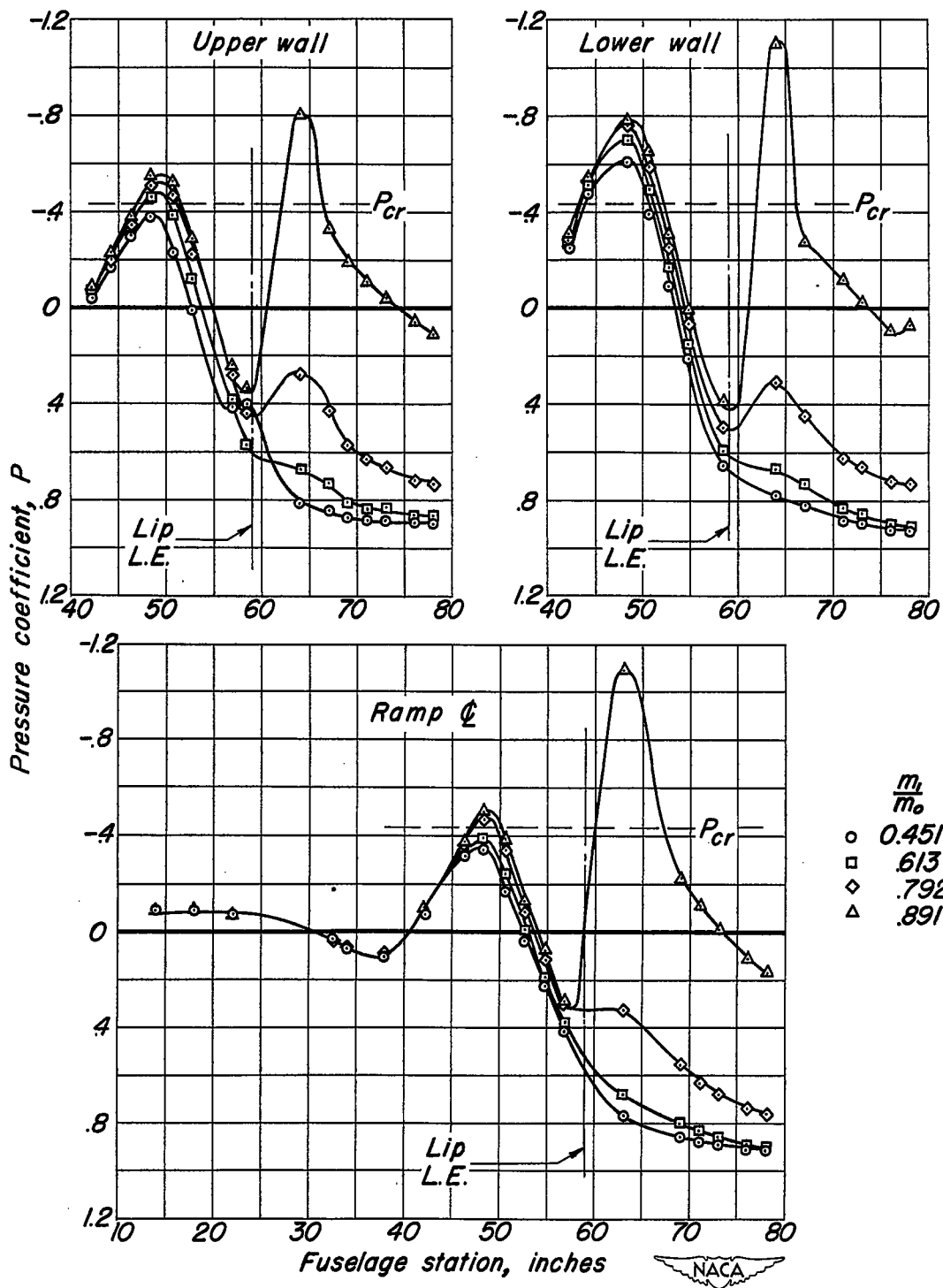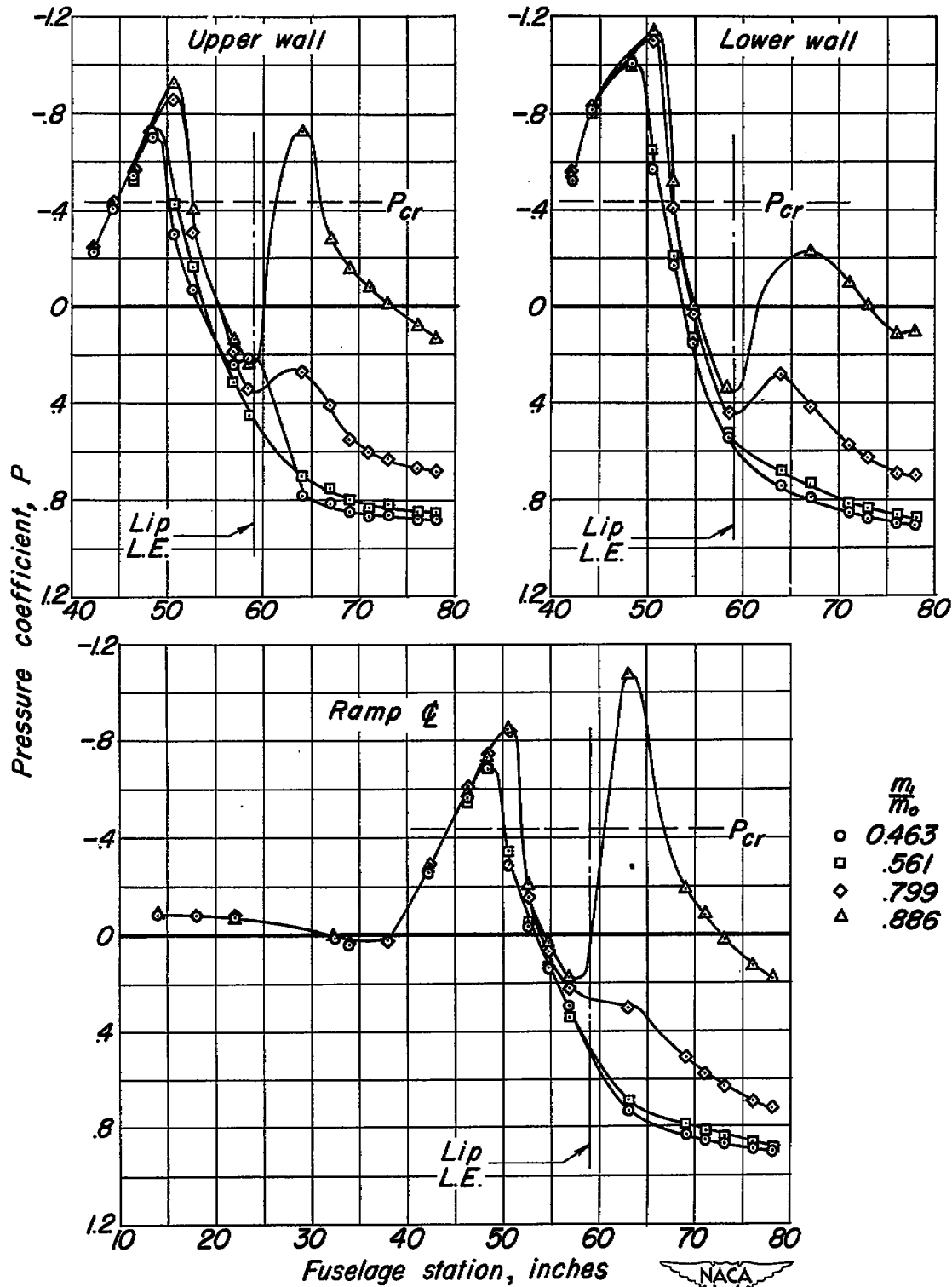
36

Figure 19.—Pressure distribution along the ramp center line, upper
and lower walls of the ramp, and inside the inlet. M_o, 0.70; α_u,
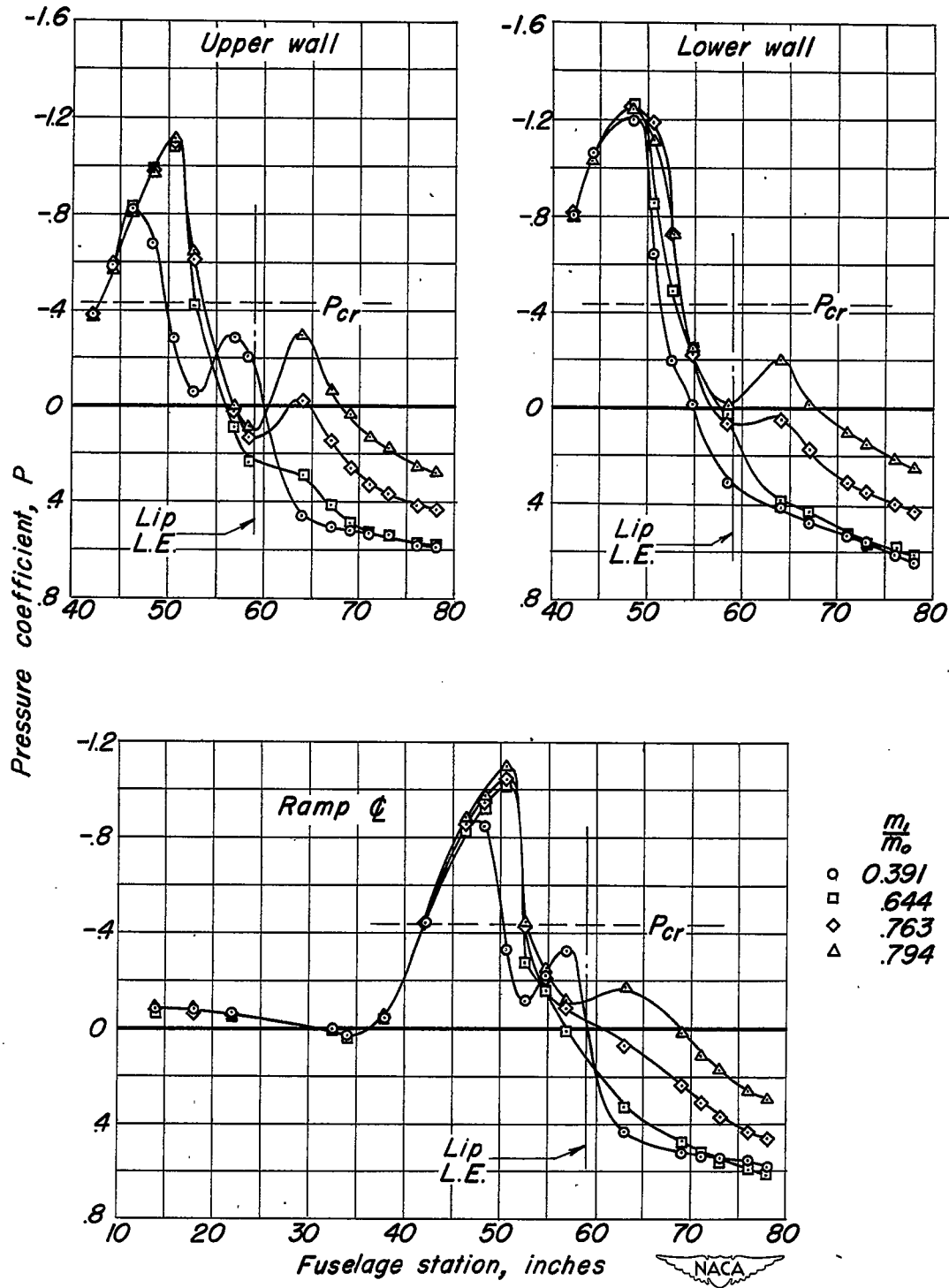6°. Inlet at station 59.00.

Figure 20.— Pressure distribution along the ramp center line, upper and lower walls of the ramp, and inside the inlet. M_o, 0.80; α_u, -2°. Inlet at station 59.00.

Figure 21.—Pressure distribution along the ramp center line, upper and lower walls of the ramp, and inside the inlet. M_o, 0.80; α_u, 0°. Inlet at station 59.00.

Figure 22.– Pressure distribution along the ramp center line, upper and lower walls of the ramp, and inside the inlet. M_0, 0.80; α_u, 2°. Inlet at station 59.00.
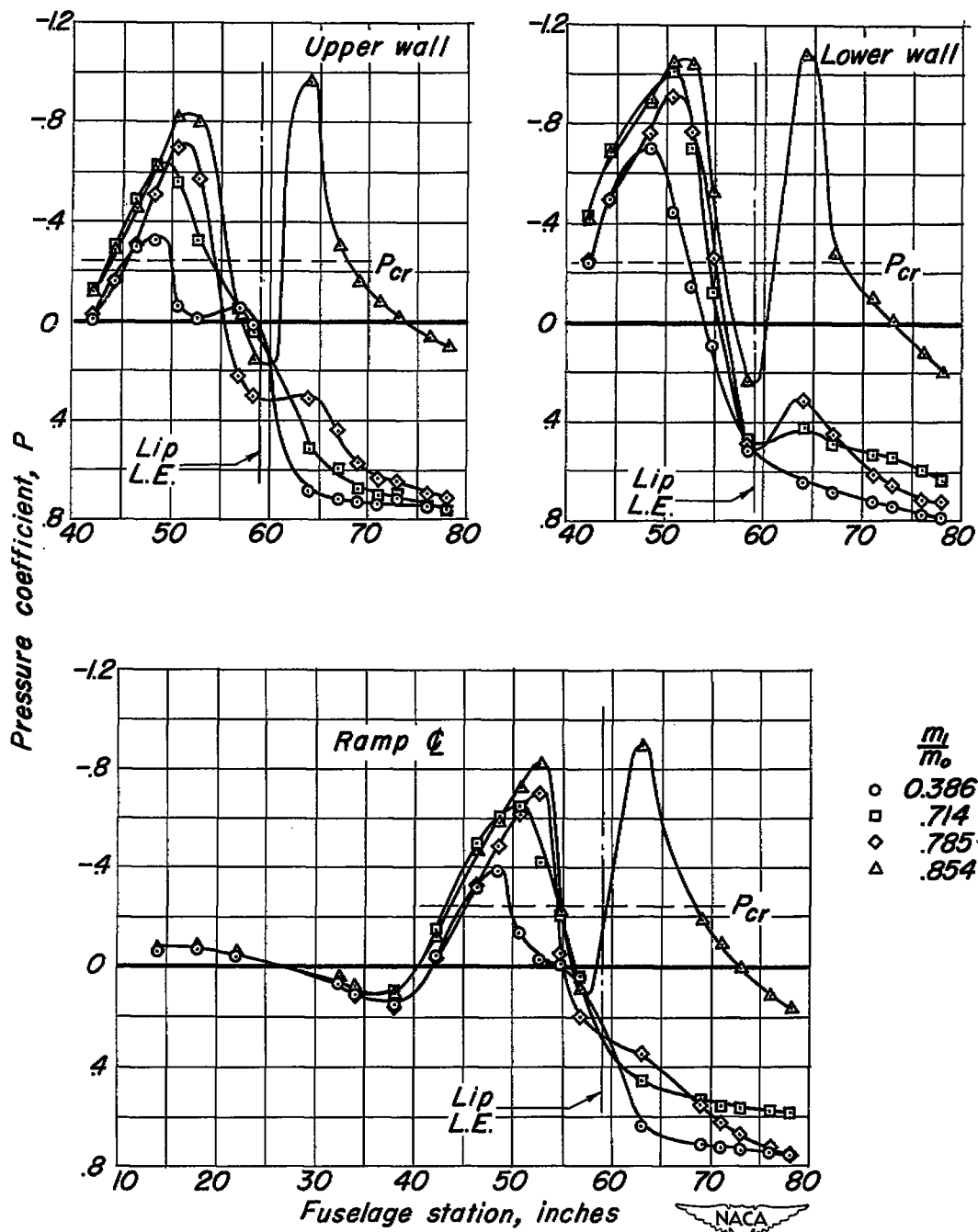
Figure 23.— Pressure distribution along the ramp center line, upper and lower walls of the ramp, and inside the inlet. M_o, 0.875; α_u, -2° Inlet at station 59.00.
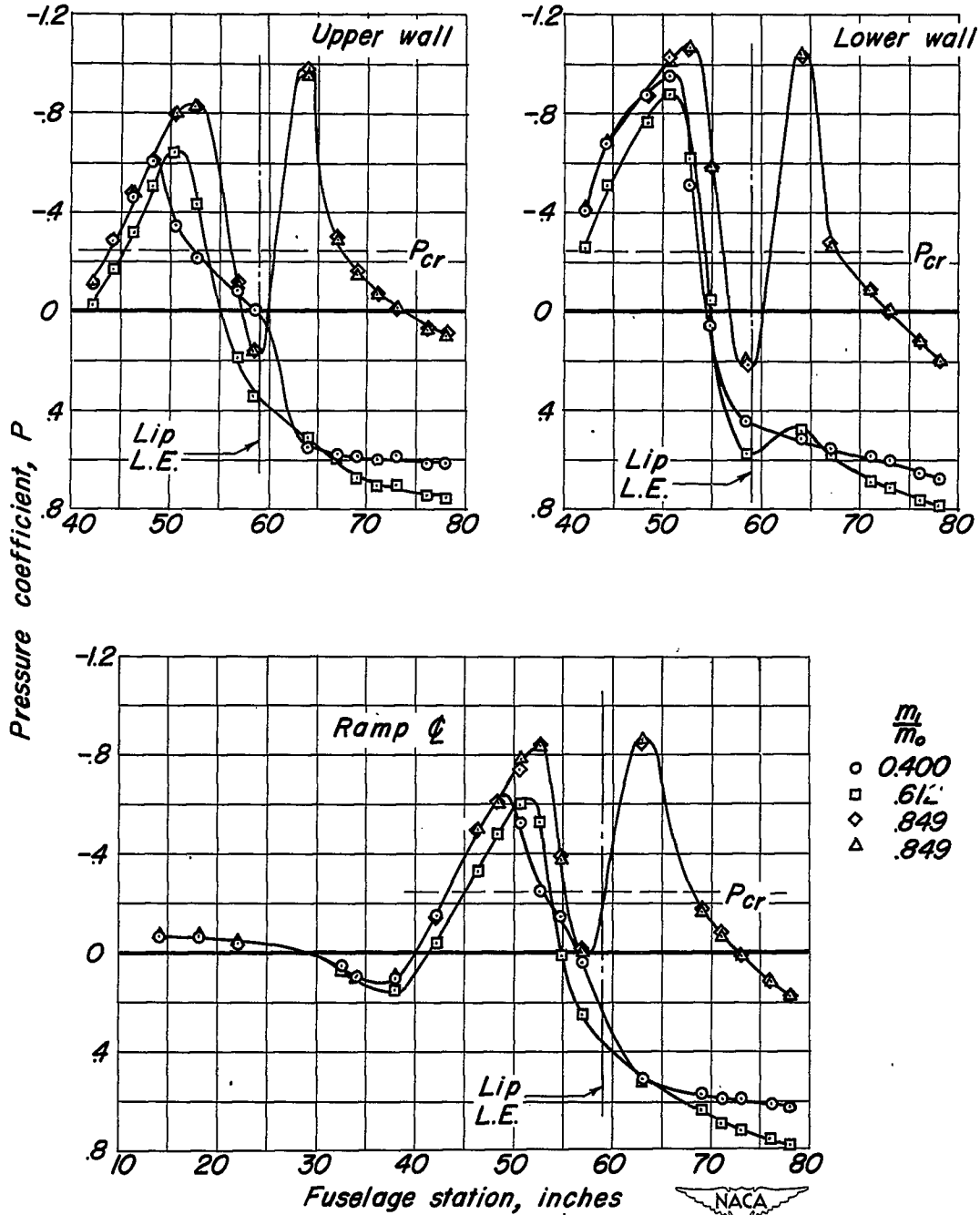
Figure 24.— Pressure distribution along the ramp center line, upper and lower walls of the ramp, and inside the inlet. M_o, 0.875; α_u, 0°. Inlet at station 59.00.